Towards Intelligent Power-System Monitoring:
Segmentation, Feature Extraction, and Identification of Underlying Causes

CUONG DUC LE

Department of Signals and Systems
CHALMERS UNIVERSITY OF TECHNOLOGY
Göteborg, Sweden 2011

Thesis for the degree of Licentiate of Engineering

Towards Intelligent Power-System Monitoring:
Segmentation, Feature Extraction, and Identification of Underlying Causes

Cuong Duc Le

CHALMERS

Signal Processing Group
Department of Signals and Systems
Chalmers University of Technology
Göteborg, Sweden 2011

Towards Intelligent Power-System Monitoring:
Segmentation, Feature Extraction, and Identification of Underlying Causes

Cuong Duc Le

This thesis has been prepared using LaTeX.

Technical Report No. R003/2011
Department of Signals and Systems
Chalmers University of Technology
ISSN 1403-266X

Signal Processing Group
Department of Signals and Systems
Chalmers University of Technology
SE-412 96 Göteborg, Sweden
Phone: +46 (0)31 772 1000

Author e-mail: cuongl@chalmers.se

Printed by Chalmers Reproservice
Göteborg, Sweden, March 2011

Abstract

The increase in size of modern power systems together with the concept smart grid requires advanced monitoring to ensure system availability, reliability, and power quality. The huge amount of available data no longer permits analysis to be implemented manually and centrally. Automatic methods are desirable to extract useful information contained in the data to help system operators follow the condition of individual devices as well as the whole system.

This thesis proposes a monitoring system structure where data is analyzed at distributed levels depending on the monitoring purpose. The system focuses on analysis of power-system events and variations captured in voltages and current waveforms. A segmentation scheme using both causal and anti-causal segmentation is developed. A method to find the optimal threshold for the detection index in the segmentation algorithm based on detection theory is also introduced. The proposed segmentation scheme and statistically-based threshold setting method are applied to a Kalman filter-based segmentation algorithm where both semi-synthetic data and real measurement data are tested. The results show that the location in time of underlying transitions in the power system is accurately estimated. The proposed segmentation method is integrated in an event monitoring system where both voltage and current waveforms are used to find the underlying cause and the location of event origin. A case study is performed on a large-scale wind park to analyze several events including faults and switching events.

Analysis of power-system data employs a number of signal-processing estimation techniques. Most of the estimation techniques are based on the assumption that the noise embedded in the observed signal is white which is not the case for power-system noise. An evaluation method is thus proposed to observe the performance of these estimation techniques under real power-system noise. The application of the evaluation method to a number of estimation techniques is shown to be feasible.

Keywords: Power-system monitoring, power-system measurement, segmentation, event analysis, signal-processing applications, harmonics analysis, power quality.

Acknowlegments

The research project associated with this thesis is sponsored by the Swedish Research Council (VR). During the working time and the writing time of this thesis, I have received uncountable help and support. I would like to take this chance to deeply thank the following people:

- my supervisor, Prof. Irene Gu, for her enthusiastic and patient supervision as well as valuable technical advices during the work.
- my co-supervisor, Prof. Math Bollen, for his excellent supervision, guidance, and encouragement. His help goes beyond the scope of power-engineering knowledge.
- Prof. Mats Viberg, head of the Signal Processing group, for creating a wonderful research environment in the group.
- Sarah Rönnberg, Mats Wahlberg, and Kai Yang at Electric Power Engineering, Luleå University of Technology, for their kind help with measurement data.
- Dr. Tuan Le at Electric Power Engineering, Chalmers University of Technology, for sharing his valuable experience of being a PhD student.
- the members of the Signal Processing group for their kind help and interesting social activities: coaching and kickoff.
- my friends for their friendship making my life much more joyful.
- my great family members for their continuous non-technical support and encouragement.

Cuong Le
Göteborg, March 2011

List of Publications

The thesis is based on the following publications

Paper A
C. D. Le, M. H. J. Bollen, and I. Y. H. Gu, "Analysis of power disturbances from monitoring multiple levels and locations in a power system," in *Proceedings of* 14^{th} *International Conference on Harmonics and Quality of Power (ICHQP)*, Bergamo, Italy, September 2010.

Paper B
C. D. Le, I. Y. H. Gu, and M. H. J. Bollen, "A new accurate segmentation scheme for power-system disturbance recordings," submitted to *IEEE Transactions on Instrumentation and Measurement*.

Paper C
C. D. Le, M. H. J. Bollen, and I. Y. H. Gu, "A method to evaluate harmonic model-based estimations under non-white measured noise," preliminarily accepted, *IEEE Power Engineering Society PowerTech Conference*, Trondheim, Norway, June 2011.

Other publications by the author, omitted in the thesis

C. D. Le, I. Y. H. Gu, and M. H. J. Bollen, "Joint causal and anti-causal segmentation and location of transitions in power disturbances," in *Proceedings of IEEE Power and Energy Society General Meeting*, Minneapolis, US, July 2010.

C. D. Le and M. H. J. Bollen, "Ride-through of induction generator based wind park with switched capacitor, SVC, or STATCOM", in *Proceedings of IEEE Power and Energy Society General Meeting*, Minneapolis, US, July 2010.

Contents

Part I
Introduction

Chapter 1

Introduction

1.1 Background

Modern electric power systems with higher penetration of new distributed power sources such as wind power and solar power have seen the participation of a large amount of new power electronic devices. The recently developed technology related to the concept "*smart grid*" in power systems also contributes to make the system more complex. Together with the growth in population of these primary devices, a great number of measuring and monitoring devices from revenue meters through protection relays to digital fault recorders have been installed at multiple locations and voltage levels in the power system for monitoring purposes. All of these secondary devices possess the ability to capture and store disturbance waveforms. The lack of automatic analysis methods, however, makes it difficult to fully exploit the useful information contained in these captured data. By applying appropriate processing methods, information about the underlying cause of the disturbance and its origin can be obtained and used for system maintenance and healing. Thus, it is needed to develop a monitoring system with the following essential automatic functions:

- Collect power disturbance data (voltage and current) from multiple monitoring points.
- Analyze the acquired data to extract features.
- Classify the disturbances according to their underlying causes based on the obtained features.

- Interpret the obtained information into handy forms used by system and network operators for example for monitoring and maintenance purposes.

To develop such a system, it is required among others development of the following signal-processing tools:

- ***Segmentation:*** To partition the disturbance data sequences into event segments and transition segments. Different signal-processing techniques are required for different types of segments due to the difference in the waveform characteristics (stationary and non-stationary).
- ***Feature extraction:*** To extract all underlying information that characterizes the disturbances and to select appropriate features.
- ***Classification:*** To design robust classifiers to classify the disturbances according to their underlying causes based on the obtained features.

In order to develop such a system, besides a solid background of power engineering, knowledge of signal processing plays an important role. Different signal-processing techniques are employed to process and transform the input signals (i.e., voltage and current waveforms) into different domains to exploit underlying information (or features). Machine learning is also essential for classifier design.

1.2 Related Work

In this section, a review of the research topic in the literature and its remaining problems are presented. This review is dedicated to the three main subject of the research, i.e., segmentation, feature extraction, and classification.

Segmentation

According to [1], there are a number of signal-processing methods used for detection and segmentation purposes divided into three groups based on: time-dependent waveform features; high-pass or band-pass filters; and parametric models.

In the first group based on time-dependent waveform features, a number of studies have been done based on rms and amplitude values and the definition of voltage events in [2]. The basic idea is to calculate the rms/amplitude

value and then compare with a threshold based on the definition to detect the event segments. In [3] and [4], rms-based segmentation and detection methods are introduced and applied to develop an automatic classification system. A technique to track the amplitude of the voltage dip used for rapid dip detection is presented in [5]. In the second group based on high-pass or band-pass filters, wavelet filter based detection has been widely used, e.g., [6]-[8]. A method using high-pass filter technique is also introduced in [4]. Another method using high order cumulants is proposed in [9]. In the methods in the last group based on parametric models, a model is employed to estimate the signal. The large model unfit caused by abrupt changes in the signal is used as an indication signal for the presence of a transition segment. In power engineering, the harmonic model is widely employed in a number of estimation techniques, e.g., Kalman filter, MUSIC (Multiple Signal Classification), and ESPRIT (Estimation of Signal Parameters via Rotational Invariance Techniques) [10]-[13]. Kalman filters have been shown to have very good performance and suitable for real-time applications with the presence of measurement noise [14]. Part of the work in [15] has proposed a segmentation method based on Kalman filtering. Another example of Kalman filter application to detect and analyze voltage events is presented in [16].

To summarize, there are a number of studies on the segmentation problem using various signal-processing techniques, of which the Kalman filter-based and the rms-based methods are found to be most robust [17]. The rms-based method is straight forward but the limitation is the time resolution.

Feature extraction and classification

Feature extraction and classification are two close issues. A classifier cannot work without a feature space and the feature space plays an important role on the performance of the classifier. A good feature space can give good classification results without a complex classifier. Depending on the purpose of classification, feature extraction and classification problems may be relatively simple or very complicated. For example, it is much easier to extract the features and design the classifier to distinguish between voltage dip (a drop in voltage magnitude) and voltage swell (a rise in voltage magnitude) events than to distinguish whether a voltages dip is caused by motor starting or transformer saturation. The latter case refers to classification based on underlying causes which is drawing more interests than classification based on the waveform morphology (i.e., dip, swell, or transient).

There are a number of studies on this topic using different classifiers, e.g., rule-based expert system, Artificial Neural Network (ANN), and Support Vector Machine (SVM). The rule-based system has been applied for power

disturbance classification in, e.g., [18]-[22]. In [18], a fuzzy expert system is applied to the classification of several voltage disturbances, including: dip, swell, surge, and outage. Some other works expand the use of this rule-based system to some more types of disturbance (e.g., transient) [19], [20]. There are a few works, e.g. [21] and [22], employing this rule-based system to classify disturbances based on their underlying causes, including: capacitor switching, motor starting, transformer saturation, energizing, etc.

In addition to the rule-based system, statistically based classification systems have been widely employed. Some typical applications of ANN in power systems are described in [23], including fault classification. This application of ANN can be found in a number of studies [24]-[28]. Support vector machine (SVM) [29] is another advanced statistically based classification method. SVM has been recently applied in power engineering and reported in a number of works [30]-[35]. Similar to the rule-based expert classifiers, however, most of the statistically based classifiers are still limited to classification based on waveform morphology or disturbances with quite distinct causes (e.g., disturbance due to faults and transformer energizing in [32]).

1.3 Motivation

The motivation of this thesis work is inspired from some of the non-resolved issues found in the related works on the problems of segmentation, feature extraction, and classification. The Kalman filter-based segmentation method has to cope with the problem of threshold setting for the so-called detection index. Another problem lies in the fact that there is always some detection delay due to the effect of the window used to calculate the detection index. Solving the two problems is one of the motivations of this thesis work.

From the literature, it has been seen that there are available signal-processing techniques which can be used for feature extraction and classification of power-system disturbances. However, most of the works focus on classification based on the waveform morphology which is easier but gives less useful information than classification based on underlying causes [1]. Some of the reasons that make the latter a more complicated problem are:

- The lack of labeled data: The training process of statistics-based classification methods requires a large amount of labeled data which is usually not made available by the power companies.
- The lack of efficient methods to select and extract suitable features for possible disturbances in the power systems. This has been shown to be a very challenging work.

- The lack of a framework for typical problems such as classifier design, performance evaluation, and class selection within power engineering applications. A discussion on these problems is recently initiated in [36].

Another fact is that most of the studies focus on analyzing and classifying the disturbances from a single data set. The data set is either generated from simulations or obtained from measurements at some single point in the power system. There is very limited attention to the cooperation to monitor a large system at multiple locations.

To conclude, all of the mentioned problems show that research in this area is very challenging but promising. A system which is able to automatically monitor and efficiently analyze and classify disturbances is desired once the power systems become more and more complex.

1.4 Contribution of This Thesis

Paper A: ***Analysis of Power Disturbances from Monitoring Multiple Levels and Locations in a Power System***

In this paper, we propose a system to automatically analyze and characterize all available data collected from multiple monitor points in a power system. The captured disturbances are then processed and classified according to their underlying causes. Besides classification, post-processing techniques to track the location of the source of disturbances are included in the proposed system. This paper lays a framework for our research. The proposed system is applied to a case study to monitor a large-scale wind park. A number of disturbances including fault, unit tripping, transformer, capacitor, and cable energizing are considered.

Paper B: ***A New Accurate Segmentation Scheme for Power-System Disturbance Recordings***

This paper focuses on the segmentation problem. In this paper, we propose a segmentation scheme to overcome the problem of the conventional methods, i.e., the detection delay. By using this scheme, we show that the underlying transition can be accurately estimated by combining the causal (forward) and anti-causal (backward) segmentations. Another contribution in this paper is a new statistically based method for threshold setting of the detection index used in the segmentation algorithm. The performance

of this segmentation scheme applied to a Kalman filter-based segmentation algorithm is tested against different scenarios of the point on wave, depth of transition, speed of transition, and noise level. A brief introduction to this is included in Chapter 2. Part of this work is also included in [37].

Paper C: ***A Method to Evaluate Harmonic Model-Based Estimation under Non-white Measured Noise***

Different signal-processing techniques have been applied to analyze power-system disturbances; and one category of them employ a harmonic model under which observed signals are assumed to contain different harmonics plus white noise. However, measurements show that the spectrum of power-system noise is far from that of white noise. In this paper, we introduce a method to test and evaluate the signal-processing techniques under the real power-system noise. The method is applied to evaluate some techniques usually used in power engineering, including: Kalman filter, MUSIC, ESPRIT, and the segmentation method proposed in Paper B.

1.5 Thesis Outline

The thesis is divided into two parts. Part I includes four chapters. Introduction to the research topic including a review of related works, motivation and a summary of contributions of this thesis work is presented in Chapter 1. The segmentation problem and the proposed method are summarized in Chapter 2. Chapter 3 presents the automatic monitoring and analysis of power-system disturbances. Conclusions and future work are presented in Chapter 4. Part II contained the publications of this thesis.

1.6 Research Project

This project is sponsored by the Swedish Research Council (VR) under VR grant number 621-2008-5215 and carried out at the Department of Signals and Systems, Chalmers University of Technology in cooperation with Luleå University of Technology.

Chapter 2

Segmentation and Threshold Setting

As mentioned earlier, conventional segmentation methods have to cope with the problems of detection delay and threshold setting. In this chapter, a brief review of segmentation methods is first presented. A newly proposed segmentation method namely *Joint Causal and Anti-causal Segmentation* is then described. A method for choosing the threshold for the detection index is also discussed in this chapter. Finally, a case study for a Kalman filter-based segmentation is given.

2.1 Introduction

There are two concepts that are very close to each other: triggering (or detection) and segmentation [1]. The former is to find the start and end points of an event. It is usually applied for online event detection to capture disturbance waveforms. The latter is to partition the disturbance data sequence into event segments and transition segments and usually applied in a post-processing stage to find the accurate boundaries between event segments and transition segments. Figure 2.1 shows a simple example where a voltage dip event is used to illustrate triggering and segmentation.

Looking at Figure 2.1(a), the dashed black line represents the fundamental magnitude used for triggering. The trigger points (the start and end points of the voltage dip event) represented by the two solid black lines are the points at which the fundamental magnitude is equal to the threshold (represented by the horizontal dotted line). The aim of triggering is to determine these two trigger points while the aim of segmentation is to find the boundaries of the two transition segments (represented by the two green rectangles). Segmentation hence divides the disturbance recording into three

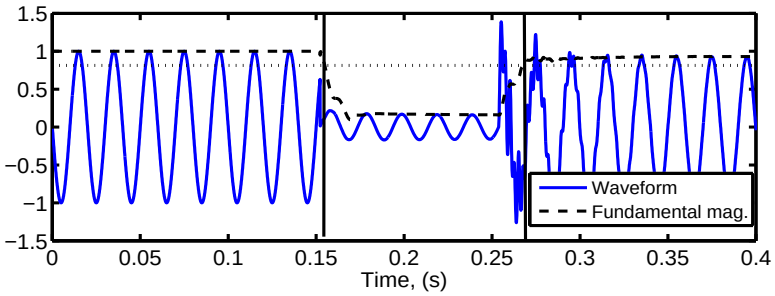

(a) Triggering with two trigger points (solid black lines)

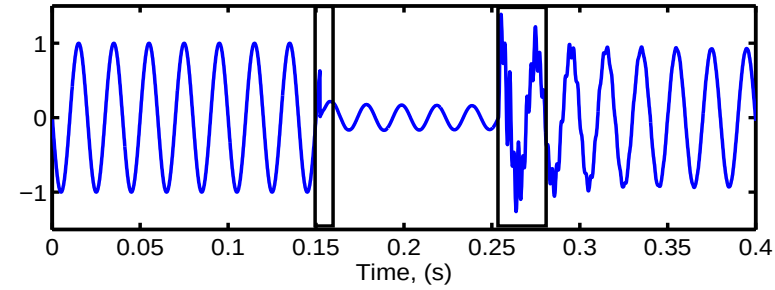

(b) Segmentation with two transition segments(solid black rectangles)

Figure 2.1: Illustration of triggering and segmentation.

event segments (before, during, and after the dip) and two transitions segments as illustrated in Figure 2.1(b).

2.2 Causal and Anti-Causal Segmentation

As previously mentioned in Section 1.3, the conventional segmentation methods have to cope with the problem of detection delay. This leads to the fact that in the case of fast transition, the underlying transition point does not lie in the detected segment as illustrated in Figure 2.2. This is due to the causality of the filter.

A *joint causal and anti-causal (CaC) segmentation* method is proposed to overcome this problem. The basic idea is to apply a joint segmentation scheme using a causal (forward time) analysis window plus an anti-causal (backward time) analysis window. This joint scheme can be applied to any type of segmentation method which is based on either time-dependent waveform features, high-pass/band-pass filters, or parametric models. Based on the results from the two analysis windows, an accurate time allocation of the underlying transition is then obtained.

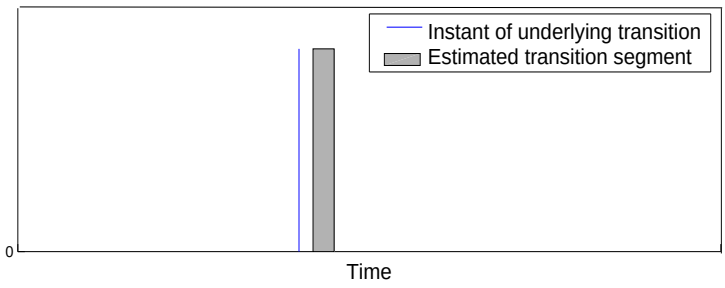

Figure 2.2: Example of conventional segmentation. The detected transition segment (grey segment) does not contain the actual transition point (blue line).

Assume that a transition from one state to another stage takes place in a time duration of D_0 as represented by a transition of a voltage signal in the top plot of Figure 2.3. The aim of the CaC segmentation is to allocate this duration.

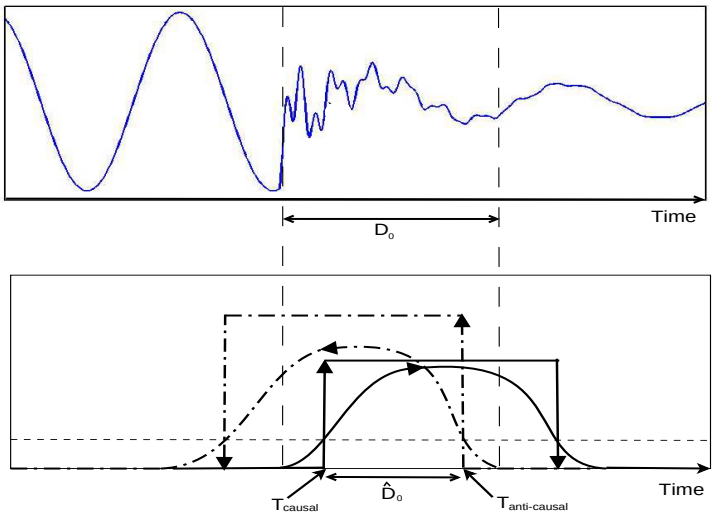

Figure 2.3: Illustration of CaC segmentation for a slow transition.

In the bottom plot of Figure 2.3, the causal (or forward) detection index (the red curve) starts increasing at the beginning of the transition. When the causal detection index crosses the threshold (the horizontal dashed black line), a causal indication flag (the red square wave) is triggered. This causal flag is reset when the causal detection index drops below the threshold. A similar process takes place in the opposite time direction (i.e., backward or

anti-causal) and an anti-causal flag is obtain. Combining these two causal and anti-causal flags (the overlap between them) results in the final estimate of the underlying transition:

$$\hat{D}_0 = [T_{causal}, T_{anti-causal}] \tag{2.1}$$

where T_{causal} and $T_{anti-causal}$ are the trigger time instants of the causal and anti-causal flags. The shorter the duration of the underlying transition, the shorter the overlap between the two flags.

When the duration of the underlying transition decreases towards a single time instant T_0 (i.e., from a slow towards a fast transition), the overlap between the two flags no longer exists. There is, instead, a gap between them as shown in Figure 2.4. The middle point of this gap is used as an estimate of the instant of the underlying transition T_0:

$$\hat{T}_0 = \frac{T_{causal} + T_{anti-causal}}{2} \tag{2.2}$$

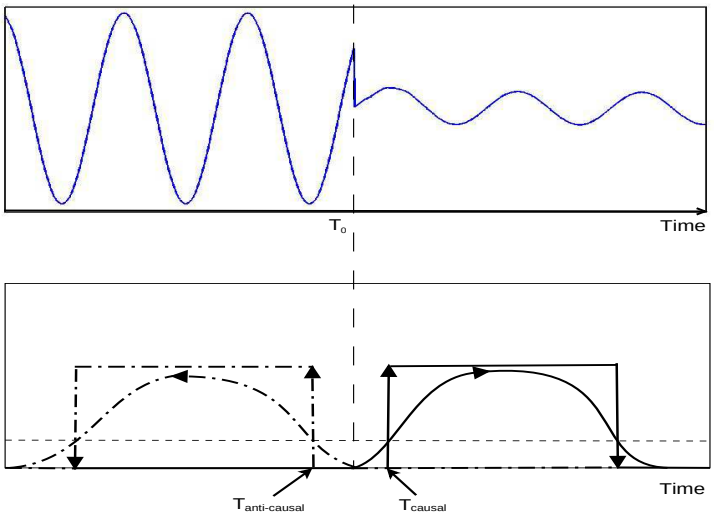

Figure 2.4: Illustration of CaC segmentation for a fast transition.

The CaC segmentation algorithm is summarized as:

- If $T_{causal} < T_{anti-causal}$, then the transition is considered as slow. The estimated duration of the underlying transition is the duration of this overlap, $\hat{D}_0$, defined by (2.1).
- If $T_{causal} > T_{anti-causal}$, then the transition is considered as fast. There is a gap between the causal and anti-causal flags. The time location of

the underlying transition is estimated as the middle point of this gap, $\hat{T}_0$, defined by (2.2).

2.3 Threshold Setting

The optimal threshold for the detection index can be determined by using the *Neyman-Pearsson* criterion [38] that maximizes the *probability of detection* under the *false alarm rate* constraint. Let di_0 and di_1 be the corresponding detection indices for the normal operation segments and the transition segments, respectively. Let the two hypotheses be:

$$\begin{cases} \bullet\ \mathcal{H}_0(\textit{null hypothesis}) : di = di_0, di_0 \sim p(di \mid \mathcal{H}_0) \\ \quad \text{(is not a transition segment)} \\ \\ \bullet\ \mathcal{H}_1(\textit{alternative hypothesis}) : di = di_1, di_1 \sim p(di \mid \mathcal{H}_1) \\ \quad \text{(is a transition segment)} \end{cases}$$

where $p(di \mid \mathcal{H}_0)$ and $p(di \mid \mathcal{H}_1)$ are the probability density functions of di under *null hypothesis* and *alternative hypothesis*, respectively. And define the following probabilities:

- $P(\alpha_i; \mathcal{H}_j)$: probability of deciding α_i corresponding to hypothesis $\mathcal{H}_i$ when hypothesis $\mathcal{H}_j$ is true.
- $P_{FA} = P(\alpha_1; \mathcal{H}_0)$: *Type I error* probability, or probability of *false alarm*.
- $P_M = P(\alpha_0; \mathcal{H}_1)$: *Type II error* probability, or probability of *miss*.
- $P_D = P(\alpha_1; \mathcal{H}_1) = 1 - P_M$: probability of *detection*.

In order to find the optimal threshold, we have to estimate the probability density function (pdf) of di during the normal operation segments ($p(di \mid \mathcal{H}_0)$) and the pdf of di during the transition segments ($p(di \mid \mathcal{H}_1)$) as illustrated in Figure 2.5 and apply the *Neyman-Pearson* approach.

The *Neyman-Pearson* approach maximizes the probability of *detection* (P_D) for a given constraint on the maximum *false alarm* $P_{FA} = \alpha$. The decision is α_1 if:

$$L(di) = \frac{p(di \mid \mathcal{H}_1)}{p(di \mid \mathcal{H}_0)} > \gamma \tag{2.3}$$

where $L(di)$ is known as the *likelihood ratio* and the *threshold* γ is found from:

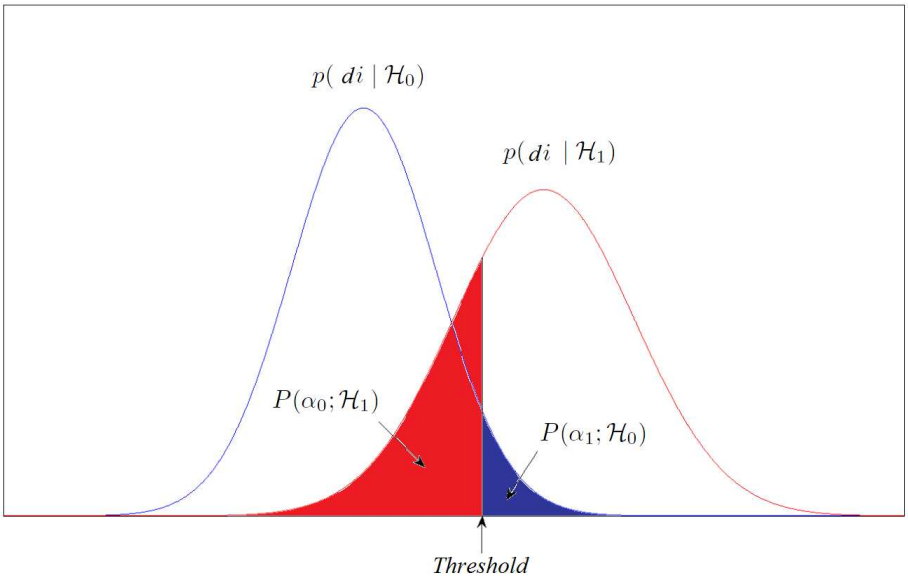

Figure 2.5: pdfs for two hypotheses. Blue area: *Type I error* probability, or probability of *false alarm*, red area: *Type II error* probability, or probability of *miss*.

$$P_{FA} = \int_{\{di:L(di)>\gamma\}} p(di \mid \mathcal{H}_0)\mathrm{d}(di) = \alpha \tag{2.4}$$

Based on this approach, given the pdfs $p(di \mid \mathcal{H}_0)$, $p(di \mid \mathcal{H}_1)$, and the *false alarm* constraint α, the *threshold* γ for the detection index di can be determined.

2.4 Kalman filter-based CaC Segmentation

The proposed CaC (Causal and Anti-Causal) segmentation and the statistically based threshold setting method are applied to a Kalman filter-based segmentation algorithm. In this segmentation algorithm, a harmonic model where a signal is modeled as the sum of M harmonics plus white noise as expressed in (2.5) is employed.

$$y(n) = \sum_{m=1}^{M} s_m(n) + v(n) = \sum_{m=1}^{M} A_m e^{j\omega_m n} + v(n) \tag{2.5}$$

Under this model, the Kalman filter is described by a set of state-space equations which are called *state equations* and *observation equations*. For a

scalar measurement data $y(n)$ modeled as in (2.5), the set of *state equations* and *observation equations* are given in (2.6) and (2.7), respectively.

$$\begin{bmatrix} s_{1,r}(n) \\ s_{1,i}(n) \\ \vdots \\ s_{M,r}(n) \\ s_{M,i}(n) \end{bmatrix} = \mathbf{A} \begin{bmatrix} s_{1,r}(n-1) \\ s_{1,i}(n-1) \\ \vdots \\ s_{M,r}(n-1) \\ s_{M,i}(n-1) \end{bmatrix} + \frac{\omega(n)}{2M} \begin{bmatrix} 1 \\ 1 \\ \vdots \\ 1 \\ 1 \end{bmatrix} \tag{2.6}$$

$$y(n) = [1\ 0\ \ldots\ 1\ 0] \begin{bmatrix} s_{1,r}(n) \\ s_{1,i}(n) \\ \vdots \\ s_{M,r}(n) \\ s_{M,i}(n) \end{bmatrix} + v(n) \tag{2.7}$$

where

$$\mathbf{A} = \begin{bmatrix} \cos\omega_1 & -\sin\omega_1 & 0 & \ldots & 0 & 0 & 0 \\ \sin\omega_1 & \cos\omega_1 & 0 & \ldots & 0 & 0 & 0 \\ \vdots & \vdots & \vdots & \ddots & \vdots & \vdots & \vdots \\ 0 & 0 & 0 & \ldots & 0 & \cos\omega_M & -\sin\omega_M \\ 0 & 0 & 0 & \ldots & 0 & \sin\omega_M & \cos\omega_M \end{bmatrix}$$

and $\boldsymbol{A}_m = A_m e^{j\phi_m} = A_{m,r} + jA_{m,i}$ is the complex magnitude of the m^{th} harmonic; $A_{m,r}$ and $A_{m,i}$ are the real and imaginary parts; ϕ_m is the initial phase; ω_m is the frequency, $s_m(n) = A_m e^{j\omega_m n}$ is the m^{th} harmonic signal component, $v(n)$ is the measurement noise, and $\omega(n)$ is the modeling noise, assumed to be zero mean white.

The squared mean of the residuals in an analysis window (or, the squared mean of the difference between $y(n)$ and the reconstructed signal $\hat{y}(n)$ from the model) is used as a *detection index* (*di*) [15]:

$$di(n) = \left[\frac{1}{L_W} \sum_{n-L_W+1}^{n} (y(n) - \hat{y}(n)) \right]^2 \quad n = L_W, ..., L \tag{2.8}$$

where $\hat{y}(n)$ is the reconstruction of $y(n)$; L_W is the analysis window length; L is the length of $y(n)$. This detection index is compared with a threshold to decide whether to trigger or to reset the transition indication flag. The algorithm is applied in both causal and anti-causal time directions as described previously in Section 2.2. Figure 2.6 shows an example of this Kalman filter-based CaC segmentation applied to a disturbance recording obtained from a 130-kV grid.

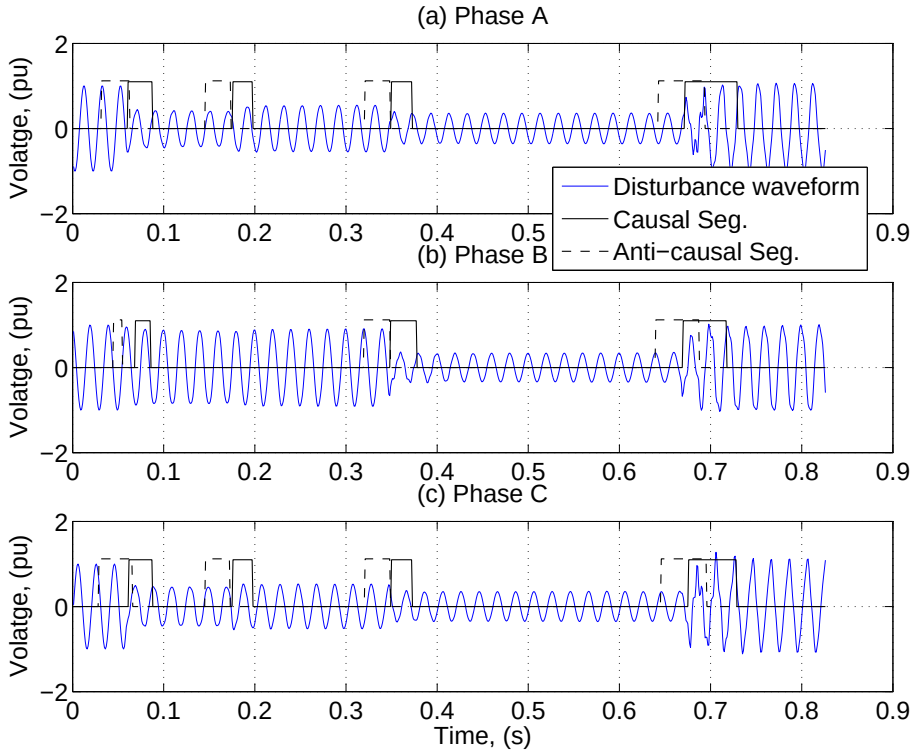

Figure 2.6: Kalman filter-based CaC segmentation for a three-phase disturbance recording obtained from a 130-kV grid.

Observing the first transition, segmentation algorithm results:

- Phase A: $T_{causalA} = 61\,\text{ms}, T_{anti-causalA} = 62\,\text{ms}$ (one sample overlap).
- Phase B: $T_{causalB} = 70\,\text{ms}, T_{anti-causalB} = 54\,\text{ms}$ (no overlap, the middle point locates at 62 ms).
- Phase C: $T_{causalC} = 62\,\text{ms}, T_{anti-causalC} = 65\,\text{ms}$ (3 samples overlap).

There are overlaps in the causal and anti-causal flags for phase A and phase C. The transition is found to start somewhere at or before 61 ms for phase A and 62 ms for phase C. Further, the middle point of the gap between the two flags in phase B locates at 62 ms. From these results, it is concluded that the underlying transition takes place at 62 ms. This transition indicates a fault inception between phase A and phase C. Phase B is not involved in the fault but the disturbance is still observed. The second transition is shown to occur at 174 ms for both phase A and phase B. The transition is likely

caused by a fast tripping of a line feeding the fault which leads to a slight voltage recovery. The transition is so small that it cannot be detected in phase B. The third transition shows that phase B quickly gets involved in the fault at 349 ms (this fast transition is observed at the same time instant for the three phases). The last transition is a slow transition, estimated to start at 672 ms, 670 ms, and 676 ms and end at 693 ms, 687 ms, and 695 ms for phases A, B, and C, respectively. The values of starting time and ending time are slightly different for the three phases but they all consistently show a slow voltage recovery in about 1 cycle followed by fault clearing. This time difference is likely due to the difference in circuit-breaker opening instants for the three phases [39].

Chapter 3

Automatic Monitoring and Analysis of Power-system Disturbances

As mentioned in Chapter 1, the large-scale power system nowadays requires a monitoring system that is able to automatically analyze the disturbances and return information in a handy form to the system operators for monitoring and maintenance purposes. In addition, the transition of the power system into the era of "*smart grid*" requires advanced monitoring and analysis of disturbances to improve system security and availability. Such monitoring systems give benefits not only in technology but also in economics. Every year, power interruptions cost, for example, the US economy from $25 to $180 billion on average [40]. If there exists a monitoring system that is able to quickly analyze and inform the system operators the type and the origin of the disturbances that cause interruption, interruption time will be reduced and economic gain is expected. In addition to post-processing after the occurrence of outages, early fault detecting and preventing outages are of more interests. This is known as failure diagnosis. In this chapter, in Section 3.1 we summarize the distributed event monitoring system proposed in this thesis and described in detail in Paper A. In Section 3.2 and Section 3.3, we introduce a vision towards a distributed intelligent monitoring system and its applications for smart grids.

3.1 The Proposed Event Monitoring System

In this section, we describe the main functions of the proposed power-system event monitoring system. The proposed event monitoring system consists of five stages. Event waveforms (voltage and current recordings) are collected

from different locations of a power system and fed into the segmentation algorithm. The events are first pre-classified based on the number of transition segments. The spatial zone of the event origin (i.e., the part of the power system where the event originates) is coarsely determined from voltage recordings only. Events are then further analyzed and characterized by extracting information from both voltages and currents. Finally more accurate information about the location of event origin is obtained by different techniques depending on the type of events. The block function diagram of the monitoring system is presented in Figure 3.1.

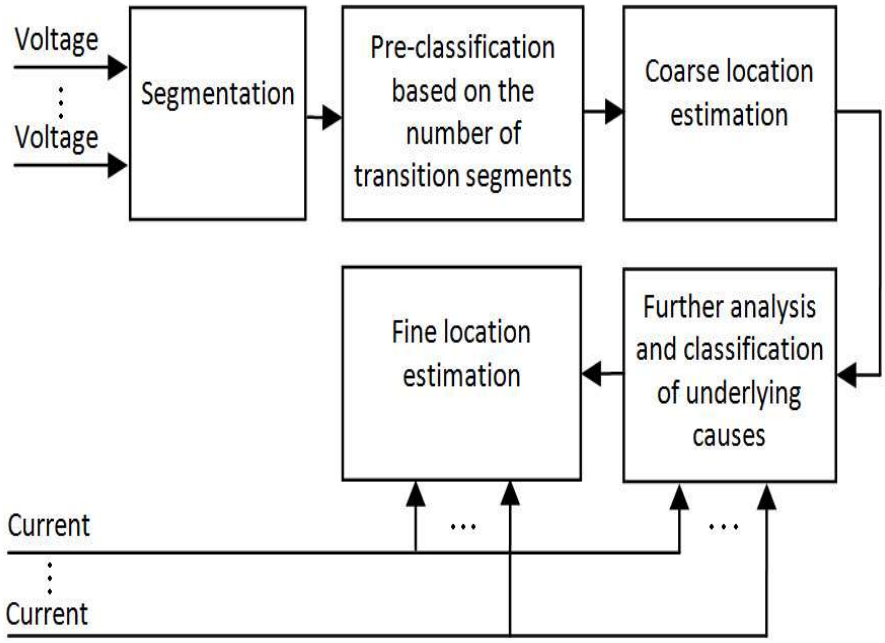

Figure 3.1: The event monitoring system.

The main functions of each stage are described as follows.

Segmentation

In this stage, voltage event recordings obtained from different monitors are segmented into transition segments and event segments based on the joint causal and anti-causal segmentation method proposed in Chapter 2.

Pre-classification

Once the number of transition segments is determined, several underlying causes of events can be roughly classified. For example, fault events consist of more than one transition segments: two for faults resulting in a single stage voltage dip and more for faults resulting in a multi-stage voltage dip. Other events such as tripping or energizing consist of only one transition segment.

Coarse location estimation

In parallel to pre-classification, the location of the event origin in relation to the position of the monitors is coarsely estimated based on the maximum detection index obtained from the segmentation stage. The aim of coarse location estimation is to reduce the total number of the possible events to be classified as not all events may occur in a specific part of the power system.

Further analysis and classification

In this stage, events are further analyzed and characterized based on the properties of voltage and current recordings, the results from the previous stages, and the system information. The aims are to find effective features and to classify the events according to their underlying causes. Various studies on classification systems are reported in the literature, e.g., neural network-based classification [24]-[28], expert system [18]-[22], support vector machines [30]-[35]. These studies emphasized that robust features play an essential role on the classification performance.

Fine location estimation

Once the underlying causes are estimated, the location of the event origin is determined more accurately in the last stage based on voltage and current recordings obtained from the monitors close to the location of event origin determined in the coarse-location-estimation stage. This requires the underlying causes to be estimated in advance since different techniques are employed to estimate the location of origin for different types of events. A number of studies on tracking the origin of capacitor switching can be found in, e.g., [41] and [42]. In Paper A, we consider two types: fault and capacitive related switching (capacitor and cable switching). Our proposed method uses the information about the phase angles of the current before and during the event to estimate the relative location of fault events. For capacitive related switching events, the relative location is estimated by comparing the

initial phase angles of the fundamental and harmonic currents immediately after the triggering instant of the event.

The proposed event monitoring system is applied to a case study to monitor small system with a wind park. A number of events including fault, unit tripping, transformer, capacitor, and cable energizing are considered.

3.2 Distributed Intelligent Monitoring System

The large size of the power system nowadays no longer permits the whole monitoring process to be implemented in a single central unit. Instead, monitoring is preferably conducted in a distributed manner, resulting in a *distributed monitoring system* [43]. In this distributed monitoring system, the tasks are divided for different monitoring levels. An example of distributed monitoring is: Local monitoring collects, stores, and preliminarily classifies to prioritize event recordings obtained from the sensors; important events are then sent to the central monitoring for further analysis to avoid unnecessarily transmitting a huge amount of data. In addition to event analysis and classification, there are a number of other functions that can exploit the information from the large number of available data, for example, variation analysis, trend analysis, and trend-deviation analysis as described in Section 3.3. The final objectives of this intelligent monitoring system are to continuously monitor the power system, to provide network operators with useful information about the disturbances, and to assess the health of the system in terms of availability, reliability and power quality. An example of the structure of such a distributed intelligent monitoring system is shown in Figure 3.2.

The monitoring system is divided into three levels, namely field level, distributed level, and central level. In such a multi-level system, communication plays an important role. Two-way communication is established to connect the local monitors with their nearby sensors and with the central monitor to ensure information exchange among the devices and to communicate with neighbor systems.

Field Monitoring

At this monitoring level, sensors play an important role of capturing the system information (voltages and currents). Sensors are for example current and potential transformers normally associated with various types of intelligent electronic devices (IEDs) present in the power system, for example, smart

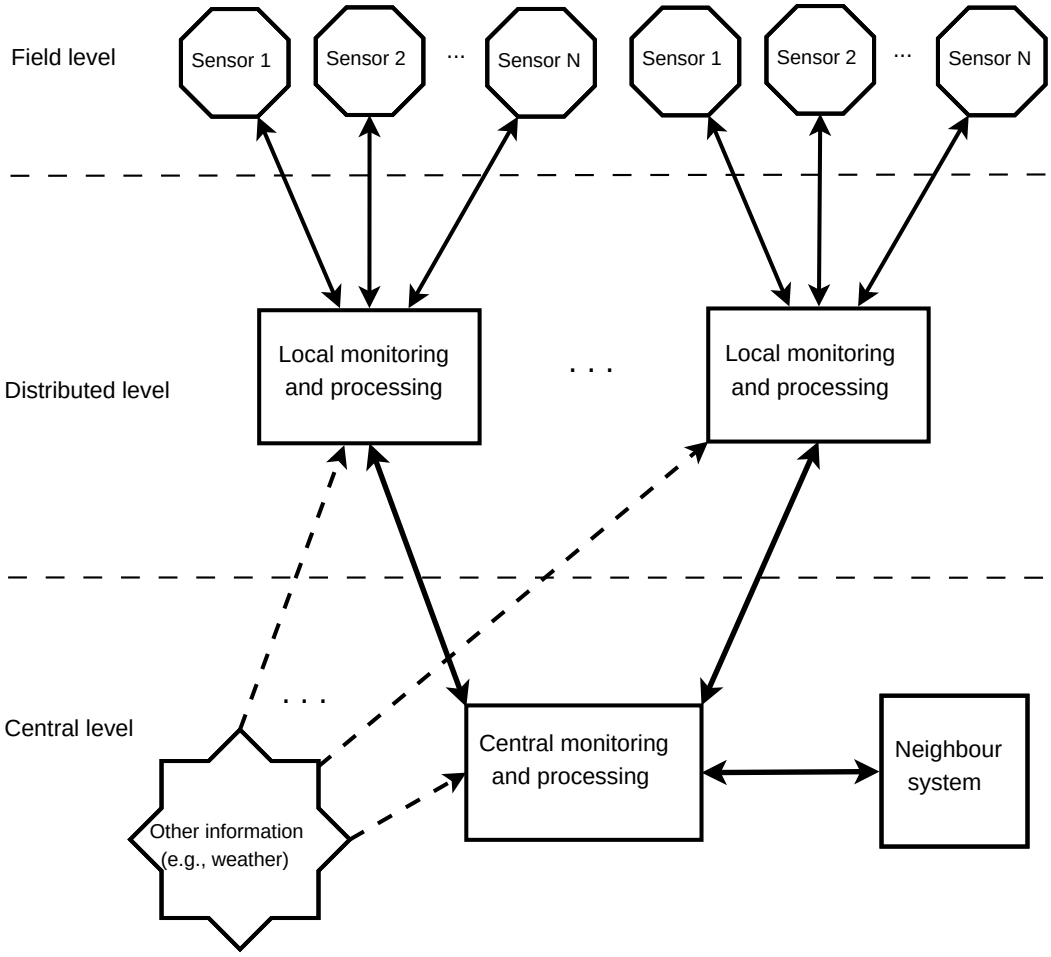

Figure 3.2: Structure of an intelligent distributed monitoring system.

meters, protection relays, digital fault recorders, and remote terminal units to convert analog signals into digital signals. At this level, signal-processing techniques like triggering and sampling are employed to capture, digitalize, and store data. Based on the type of sensor, some will obtain waveform features over pre-defined periods (e.g., the hourly energy flow for smart meters of the current generation; every second may be in a few years time) where others will only store data when a significant deviation from the normal waveform occurs (like fault recorders). There will also be special sensor that do both, like phasor measurement units (PMUs) that give phasor voltage (magnitude and phase angle) and frequency every 20 ms. The data is then used as the input for various algorithms depending on the function of the IEDs (for example, calculate impedance in distance protection relays, calculate energy in revenue meters). Data sequences associated with power-system events are

stored for further analysis at higher monitoring levels.

Distributed Monitoring and Processing

Local monitoring collects data from the nearby sensors for further analysis. One of the functions of local monitoring is, for example, to primarily classify the disturbance waveforms obtained from the sensors at the field monitoring level (e.g., classify variation and event, fault event and switching event). Each sensor may be triggered and capture a large amount of data every day. However, not all of these data are of interests. A sensor, for example, may be triggered by a normal switching of a feeder or a failure of cable insulation causing over-current. The later event is more interesting to network operators and a high priority should be given. Lower priority events may be discarded or statistics could still be kept but no details to reduce memory demand and pressure on the communication system. The segmentation and classification algorithms may be employed at this monitoring level to prioritize and analyze the disturbances waveforms. In addition to the information in the measured voltage and current waveforms, other data sources may provide additional information for classification purposes. For example, weather information about lightning, wind, or low temperature at the time of event occurrence may be an effective feature for event classification. Another function that can be implemented at this level is to monitor/follow up the performance of the nearby devices by applying long-term trend analysis. In order to reduce the demand of data storage, non-interesting data (e.g, data associated with stable trends for a long period) can be removed. Another alternative is to only store the interesting features from the data depending on monitoring purpose.

Central Monitoring and Processing

Central monitoring is dedicated to monitor the overall system performance associated with obtaining statistics about the system. Central monitoring may share the event/variation analysis task with local monitoring depending on the amount of data to be processed. The main function of central monitoring is to obtain long-term statistic information about the health of the system including reliability, availability, power quality, etc., to help network operators on planning and expanding the system. Exchanging information with other systems (within or outside the country in large-scale interconnected power systems) is performed at this monitoring level.

3.3 Applications of Distributed Intelligent Monitoring System

In this section, a number of applications of the intelligent monitoring system are presented. The applications are based on different analysis methods applied to different types of disturbance namely event analysis, variation analysis, and long-term trend analysis.

Event analysis

Events are large sudden changes (disturbances) with starting and ending time instants [17], for example, voltage dip, interruption. An important application of event analysis is to provide network operators with information about the underlying cause, time, and the location of event origin for maintenance or healing after fault. Different tools are employed to find this information. Segmentation/triggering is used to find the location in time of an underlying transition. Classification is used to find the underlying cause. These two tools are discussed in Chapter 1 and Chapter 2. In order to find information about the spatial location of an event, fault location techniques are applied. Works on fault location for transmission lines have been performed in many studies, e.g., [44]-[47]. Phasor measurement units (PMUs) are recently applied to fault location and reported in a number of studies [48]-[51].

In addition to fault classification and location, event analysis may be also used to follow up the performance of devices. Information about the duration of voltage dips or interruptions in fault events, for example, can be used to evaluate the performance of protection relays and switching devices. A circuit breaker should be taken out for maintenance if the difference in closing/opening time instants of three phases suddenly increases.

Variation analysis

Apart from events, variations are steady-state or quasi-steady-state disturbances that require continuous measurement, e.g., frequency variation, voltage magnitude fluctuations and flicker severity, and harmonic distortion [17]. Tracking of flicker or harmonics to obtain power disturbance load flow allows identifying their origin sources and appropriate mitigating solutions are then implemented. Analyzing the correlation between harmonic current and voltage at a location gives information about the harmonic impedance. This in turn provides information about the nonlinear load to control the amount of nonlinear-load-based equipment that can be connected to the system at the monitoring location.

Long-term trend analysis

Long-term trend analysis can be applied to both events and variations to follow up the operation conditions of individual devices as well as for the system as a whole. Long-term trend analysis deserves it own values of early predicting failures and assess the health of the system. A sudden change in the trend likely implies something is happening with the supervised device. The trend of partial discharge, for example, is an index for the health of insulation. A sudden increase in partial discharge frequency and level gives an alarm for network operators to apply appropriate solutions to prevent possible insulation breakdown which may lead to supply interruption. This type of trend analysis can be applied to improve system reliability by early detecting, locating, and repairing incipient failures before catastrophic failure [52].

In addition to system-reliability improvement, long-term trend analysis can be also employed to assess power quality. Processing data in a long term to obtain statistics of power quality indices, e.g., total harmonic distortion (THD), waveform distortion ratio (WDR), and symmetrical components deviation ratio (SDR) [53] can help networks operators to plan the system to meet requirement on power quality. Statistics on the number of events per year can be used to quantify the system availability.

Chapter 4

Conclusion and Future Work

4.1 Conclusion

In this thesis we propose a system to automatically analyze and classify power-system events. The system consists of five stages and focuses on three main problems (i.e., segmentation, feature extraction, and classification) which lay a framework for our research. In the system, both voltage and current recordings from different locations in the system are collected and analyzed to exploit the underlying information. The detailed system with a case study is presented in Paper A.

A segmentation method namely *joint causal and anti-causal segmentation* has been developed and shown to be able to segment disturbance waveforms with very high time resolution. The method overcomes the detection-delay problem of the conventional methods by combining both forward (causal) segmentation and backward (anti-causal) segmentation to estimate the final transition segments. The method has been shown to give very good performance under various scenarios, e.g., depth of transition, speed of transition, and noise level. Another problem of segmentation, the threshold setting, is also studied. Most segmentation methods use a so-called detection index function and a threshold to decide the trigger points of transition segments. Setting this threshold is not straightforward as it implies a trade-off between the detection rate and the false alarm rate. We propose a statistically based method to find the optimal threshold based on detection theory. The method uses the Neyman-Pearson criterion which maximizes the probability of detection under the constraint of false alarm to calculate the threshold. The segmentation and the threshold setting method are presented in Paper B.

In the proposed system, signal processing plays an important role as its techniques are employed to extract the underlying information in the distur-

bance data. The model-based techniques are based on the assumption that the noise embedded in the observed signal is white; which is not the case for the power-system noise. In order to evaluate these techniques under non-white measured noise, we propose an evaluation method using semi-synthetic data. This semi-synthetic data is obtained by embedding synthetic signals with predefined parameters into the noise sequences obtained from various power-system measurements. The performance of estimation techniques under measured noise is evaluated in a statistical sense. This evaluation method is presented in Paper C.

4.2 Future Work

Towards a complete event monitoring system in Section 3.1, there are still various challenging works, especially feature extraction and classification. In addition, accurately locating disturbance origin is an important task as it contributes to shorten interruption time caused by disturbances. A non-technical but very necessary task is to collect and label measured disturbance data as statically based classification methods require a large amount of labeled disturbance data for training. Obtaining these disturbance data is not an easy task since it is not usually made available by the power companies. Labeling the data is, however, even more challenging as disturbance data is usually captured automatically without the knowledge of what really happens in the power system. The next step of the research is to work on the disturbance data including selecting the disturbance classes to be studied, characterizing, and labeling them. It is desired to have real measured disturbance recordings but initially starting with synthetic data is a parallel alternative to develop efficient feature extraction methods. Once efficient feature extraction methods are developed, the next step is to design robust classifiers. It is also interesting to look at the problem of tracking the origin of disturbances in a meshed network which is believed to have valuable practical applications. The final objectives of the research would be the accurate answers to the questions: ***"What is the underlying cause?"*** and ***"Where and when does it happen?"***.

In addition to the event monitoring system, developing such distributed monitoring systems as described in Section 3.2 and Section 3.3 is an important step towards intelligent monitoring for smart grids. The analysis is focused on event, variation, and long-term trend analysis. To develop this requires, beyond knowledge of power engineering and signal processing, active participation from other research areas on database management, industrial communication systems, and machine leaning.

Bibliography

[1] M. H. J. Bollen, I. Y. H. Gu, S. Santoso, M. F. Mcgranaghan, P. A. Crossley, M. V. Ribeiro, P. F. Ribeiro, "Bridging the gap between signal and power: assessing power system quality using signal processing techniques," *IEEE Signal Processing Magazine*, vol. 26, no. 4, pp. 12-31, 2009

[2] M. H. J. Bollen, *Understanding power quality problems: voltage sags and interruptions*, IEEE Press, New York, 1999.

[3] E. Styvaktakis, M. H. J. Bollen, and I. Y. H. Gu, "Automatic classification of power system events using rms voltage measurements," *IEEE Power Engineering Society Summer Meeting*, 2002.

[4] T. Radil, P. M. Ramos, et al., "PQ monitoring system for real-time detection and classification of disturbances in a single-phase power system." *Instrumentation and Measurement, IEEE Transactions on*, vol. 57, no. 8, pp. 1725-1733, 2008.

[5] R. Naidoo and P. Pillay, "A new method of voltage sag and swell detection," *Power Delivery, IEEE Transactions on*, vol. 22, no. 2, pp. 1056-1063, 2007.

[6] S. Santoso, E. J. Powers, et al., "Power quality assessment via wavelet transform analysis," *Power Delivery, IEEE Transactions on*, vol. 11, no. 2, pp. 924-930, 1996.

[7] E. Perez and J. Barros, "A proposal for on-line detection and classification of voltage events in power systems," *Power Delivery, IEEE Transactions on*, vol. 23, no. 4, pp. 2132-2138, 2008.

[8] A. M. Gaouda and M. M. A. Salama, "Monitoring nonstationary signals," *Power Delivery, IEEE Transactions on*, vol. 24, no. 3, pp. 1367-1376, 2009

[9] O. N. Gerek and D. G. Ece, "Power-quality event analysis using higher order cumulants and quadratic classifiers," *Power Delivery, IEEE Transactions on*, vol. 21, no. 2, pp. 883-889, 2006.

[10] I. Kamwa, R. Grondin, et al., "On-line tracking of changing harmonics in stressed power systems: application to Hydro-Quebec network," *Power Delivery, IEEE Transactions on*, vol. 11, no. 4, pp. 2020-2027, 1996.

[11] V. M. M. Saiz and J. B. Guadalupe, "Application of Kalman filtering for continuous real-time tracking of power system harmonics," *Generation, Transmission and Distribution, IEE Proceedings*, vol. 144, no. 1, pp. 13-20, 1997.

[12] A. A. Girgis, W. B. Chang, et al., "A digital recursive measurement scheme for online tracking of power system harmonics," *Power Delivery, IEEE Transactions on*, vol. 6, no. 3, pp. 1153-1160, 1991.

[13] C. J. Dafis, C. O. Nwankpa, et al., "Analysis of power system transient disturbances using an ESPRIT-based method," *IEEE Power Engineering Society Summer Meeting*, 2000.

[14] P. K. Dash, R. K. Jena, et al., "An extended complex Kalman filter for frequency measurement of distorted signals," *Instrumentation and Measurement, IEEE Transactions on*, vol. 49, no. 4, pp. 746-753, 2000.

[15] E. Styvaktakis, *Automating power quality analysis*, PhD Thesis, Chalmers University of Technology, 2002.

[16] J. Barros and E. Perez, "Automatic detection and analysis of voltage events in power systems," *Instrumentation and Measurement, IEEE Transactions on*, vol. 55, no. 5, pp. 1487-1493, 2006.

[17] M. H. J. Bollen and I. Y. H. Gu, *Signal processing of power quality disturbance*, A John Wiley & Sons, Inc., 2006.

[18] P. K. Dash, S. Mishra, et al., "Classification of power system disturbances using a fuzzy expert system and a Fourier linear combiner," *Power Delivery, IEEE Transactions on*, vol 15, no. 2, pp. 472-477, 2000.

[19] M. B. I. Reaz, F. Choong, et al., "Expert system for power quality disturbance classifier," *Power Delivery, IEEE Transactions on*, vol. 22, no. 3, pp. 1979-1988, 2007.

[20] C. Jaehak, E. J. Powers, et al., "Power disturbance classifier using a rule-based method and wavelet packet-based hidden Markov model," *Power Delivery, IEEE Transactions on*, vol. 17, no. 1, pp. 233-241, 2002.

[21] S. Santoso, J. Lamoree, et al., "A scalable PQ event identification system," *Power Delivery, IEEE Transactions on*, vol. 15, no. 2, pp. 738-743, 2000.

[22] E. Styvaktakis, M. H. J. Bollen, and I. Y. H. Gu, "Expert system for classification and analysis of power system events," *Power Delivery, IEEE Transactions on*, vol. 17, no. 2, pp. 423-428, 2002.

[23] R. Aggarwal and S. Yonghua, "Artificial neural networks in power systems. III. Examples of applications in power systems," *Power Engineering Journal* no. 12, vol. 6, pp. 279-28, 1998.

[24] A. K. Ghosh and D. L. Lubkeman, "The classification of power system disturbance waveforms using a neural network approach," *Power Delivery, IEEE Transactions on*, vol. 10, no. 1, pp. 109-115, 1995.

[25] I. Monedero, C. Leon, et al., "Classification of electrical disturbances in real time using neural networks," *Power Delivery, IEEE Transactions on*, vol. 22, no. 3, pp. 1288-1296, 2007.

[26] J. V. Wijayakulasooriya, G. A. Putrus, and P. D. Minns, "Electric power quality disturbance classification using self-adapting artificial neural networks." *Generation, Transmission and Distribution, IEE Proceedings*, vol. 149, no. 1, pp. 98-101, 2002.

[27] S. Santoso, E. J. Powers, et al., "Power quality disturbance waveform recognition using wavelet-based neural classifier. I. Theoretical foundation," *Power Delivery, IEEE Transactions on*, vol. 15, no. 1, pp. 222-228, 2000.

[28] S. Santoso, E. J. Powers, et al., "Power quality disturbance waveform recognition using wavelet-based neural classifier. II. Application," *Power Delivery, IEEE Transactions on*, vol. 15, no. 1, pp. 229-235, 2000.

[29] V. Vapnik, *Statistical Learning Theory*, Wiley, New York, 1998.

[30] L. S. Moulin, A. P. A. da Silva, et al., "Support vector machines for transient stability analysis of large-scale power systems," *Power Systems, IEEE Transactions on*, vol. 19, no. 2, pp. 818-825, 2004.

[31] R. Salat and S. Osowski, "Accurate fault location in the power transmission line using support vector machine approach," *Power Systems, IEEE Transactions on*, vol. 19, no. 2, pp. 979-986, 2004.

[32] P. G. V. Axelberg, I. Y. H. Gu, and M. H. J. Bollen, "Support vector machine for classification of voltage disturbances," *Power Delivery, IEEE Transactions on*, vol. 22, no. 3, pp. 1297-1303, 2007.

[33] L. Whei-Min, W. Chien-Hsien, et al., "Detection and classification of multiple power-quality disturbances with Wavelet multiclass SVM," *Power Delivery, IEEE Transactions on*, vol. 23, no. 4, pp. 2575-2582, 2008.

[34] B. Ravikumar, D. Thukaram, et al., "Application of support vector machines for fault diagnosis in power transmission system," *Generation, Transmission & Distribution, IET*, vol. 2, no. 1, pp. 119-130, 2008.

[35] B. Ravikumar, D. Thukaram, and H. P. Khincha, "An approach using support vector machines for distance relay coordination in transmission system," *Power Delivery, IEEE Transactions on*, vol. 24, no. 1, pp. 79-88, 2009.

[36] J. Morais, Y. Pires, et al., "A framework for evaluating automatic classification of underlying causes of disturbances and its application to short-circuit faults," *Power Delivery, IEEE Transactions on*, vol. 25, no. 4, pp. 2083-2094, 2010.

[37] C. D. Le, I. Y. H. Gu, and M. H. J. Bollen, "Joint causal and anti-causal segmentation and location of transitions in power disturbances," IEEE PES General Meeting, Minneapolis, Minnesota, USA, July 25-29, 2010.

[38] M. K. Steven, *Fundamentals of statistical signal processing - detection theory*, Prentice-Hall PTR, 1998.

[39] M. H. J. Bollen, "Voltage recovery after unbalanced and balanced voltage dips in three-phase systems," *Power Delivery, IEEE Transactions on*, vol. 18, no. 4, pp. 1376-1381, 2003.

[40] L. Peretto, "The role of measurements in the smart grid era," *IEEE Instumentation and Measurement Magazine*, pp. 22-25, 2010.

[41] S. Santoso, J. D. Lamoree, and M. F. McGranaghan, "Signature analysis to track capacitor switching performance," *Transmission and Distribution Conference and Exposition, IEEE/PES*, Atlanta, GA, USA, 28 Oct. - 02 Nov, 2001.

[42] G. W. Chang, J. P. Chao, et al., "On tracking the source location of voltage sags and utility shunt capacitor switching transients," *Power Delivery, IEEE Transactions on*, vol. 23, no. 4, pp. 2124-2131, 2008.

[43] L. Fangxing, Q. Wei, et al., "Smart transmission grid: vision and framework," *Smart Grid, IEEE Transactions on*, vol. 1, no. 2, pp. 168-177, 2010.

[44] A. A. Girgis, D. G. Hart, et al., "A new fault location technique for two- and three-terminal lines," *Power Delivery, IEEE Transactions on*, vol. 7, no. 1, pp. 98-107, 1992.

[45] L. Ying-Hong, L. Chih-Wen, et al., "A new fault locator for three-terminal transmission lines using two-terminal synchronized voltage and current phasors," *Power Delivery, IEEE Transactions on*, vol. 17, no. 2, pp. 452-459, 2002

[46] S. M. Brahma and A. A. Girgis, "Fault location on a transmission line using synchronized Voltage measurements," *Power Delivery, IEEE Transactions on*, vol. 19, no. 4, pp. 1619-1622, 2004.

[47] S. M. Brahma, "Fault location scheme for a multi-terminal transmission line using synchronized Voltage measurements," *Power Delivery, IEEE Transactions on*, vol. 20 no. 2, pp. 1325-1331, 2005.

[48] J. Joe-Air, Y. Jun-Zhe, et al., "An adaptive PMU based fault detection/location technique for transmission lines. I. Theory and algorithms," *Power Delivery, IEEE Transactions on*, vol. 15, no. 2, pp. 486-493, 2000.

[49] J. Joe-Air, L. Ying-Hong, et al., "An adaptive PMU based fault detection/location technique for transmission lines. II. PMU implementation and performance evaluation," *Power Delivery, IEEE Transactions on*, vol. 15, no. 4, pp. 1136-1146, 2000.

[50] Y. Chi-Shan, L. Chih-Wen, et al., "A new PMU-based fault location algorithm for series compensated lines," *Power Delivery, IEEE Transactions on*, vol. 17, no. 1, pp. 33-46, 2002.

[51] L. Kai-Ping, L. Chih-Wen, et al., "Transmission network fault location observability with minimal PMU placement," *Power Delivery, IEEE Transactions on*, vol. 21, no. 3, pp. 1128-1136, 2006.

[52] B. D. Russell, and C. L. Benner, "Intelligent systems for improved reliability and failure diagnosis in distribution systems," *Smart Grid, IEEE Transactions on*, vol. 1, no. 1, pp. 48-56, 2010.

[53] L. Tao and A. Domijan, "On power quality indices and real time measurement," *Power Delivery, IEEE Transactions on*, vol. 20, no. 4, pp. 2552-2562, 2005.

Part II
Included Papers

Paper A

Analysis of Power Disturbances from Monitoring Multiple Levels and Locations in a Power System

Cuong D. Le, Math H. J. Bollen, and Irene Y. H. Gu

Presented at *The 14th IEEE International Conference on Harmonics and Quality of Power*

The layout has been revised.

Abstract

This paper proposes a new methodology for diagnosing the original source and underlying causes of power system disturbances, where voltage and current recordings from different locations of a power system are collected. In the proposed method, disturbances are first preclassified based on the number of transition segments. The spatial zone of the source of disturbances is coarsely determined from voltage recordings only. Disturbances are then further analyzed and characterized by extracting information from both voltages and currents. Finally more accurate information about the location of the source of disturbances is obtained by different techniques depending on the type of disturbances. Several underlying causes are analyzed and classified by using the proposed features extracted from both voltage and current waveforms. Finally, the location of the source of disturbances is refined once the underlying causes are found. Case studies were performed on a large grid-connected wind farm with disturbances from several underlying causes, including: fault, unit tripping, transformer, capacitor, and cable energizing generated by PSCAD/EMTDC.

Keywords: Power transmission and distribution, signal-processing applications, power-system disturbances, power quality, power-system monitoring, disturbance location.

1 Introduction

Modern power systems are getting increasingly large and complex with the presence of a large number of devices. Further, many devices are available in the power system that record disturbances, from digital fault recorders through protection relays to revenue meters. The lack of automatic analysis methods makes it difficult to fully exploit the useful information from these data. Ideally, an automatic analysis system would be able to classify high percentage of disturbances (e.g., 98%) while the remaining disturbances (often important disturbances, associated with rare events) could be studied manually by power system experts. The aim of the proposed method is to automatically analyze and characterize all available data collected from different points of a power system into a central unit, and then classify these events according to their underlying causes. We introduce a new method for analyzing and classifying power quality events by using both voltage and current data from multiple locations. Some case studies are conducted on a large grid-connected wind farm as described in Appendix 7.1. Section 2 of the paper describes the overall monitoring system. In Section 3, we propose a method to find the coarse spatial zone of the source of disturbance in relation to the monitor position. Characterization for some disturbances is then presented in Section 4. In Section 5, methods to refine the location of the source of disturbances are described based on comparing the phase angles of the currents, once the underlying cause is estimated. Conclusions are given in Section 6. In the appendix, a description of the test system used to generate data for our case studies and a brief review of the segmentation method used are given.

2 General Description of The Proposed System

The proposed system consists of five stages. The first is to apply a causal and anti-causal segmentation method [1] to voltage recordings obtained from different measurement points (monitors) to find the transition segments. In the second stage, disturbances are preliminarily classified based on the number of transition segments. From the detection parameters obtained from Kalman filter residuals, a coarse estimation for the location of the source of disturbances is then implemented to determine an approximate spatial area where the source of the disturbance is most likely found. In the fourth stage, disturbances are further analyzed and classified according to their underlying causes. All available information, including system information, extracted features from voltages and currents, and results from previous stages, is used in this stage. In the last stage, a fine estimation method is applied to find more accurate location of the source of disturbances based on both voltage and current recordings from different monitors in the coarsely estimated zone. Figure 1 shows the block diagram of the proposed system.

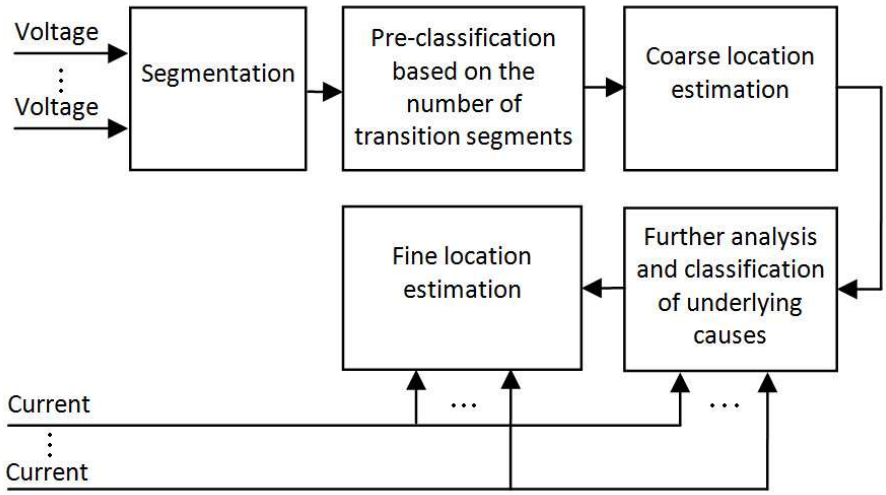

Figure 1: Monitoring system.

Segmentation

In this stage, voltage recordings from different monitors are segmented into transition and event segments, and then time synchronized based on the joint causal and anti-causal segmentation method in [1] (see the summary in Appendix 7.2). Some other segmentation methods, for example, [2] and [3], could also be applied in this step.

Pre-classification

Once the number of transition segments is determined, some underlying causes of disturbances can be roughly classified. For example, fault events consist of more than one transition segments: two for single stage faults and more for multistage faults. Other events such as tripping or energizing consist of only one transition segment.

Coarse location estimation

In parallel to pre-classification, the location of the source of disturbances in relation to the position of the monitors is coarsely estimated based on the maximum detection parameter obtained from the segmentation. The aim of this stage is also to reduce the total number of the possible events to be classified as not all events may occur in a specific part of the system. The method is described in detail in Section 3.

Further analysis

In this stage, disturbances are further analyzed and characterized based on the properties of voltage and current recordings, the results from the previous stages, and the system information. The aims are to find effective features and to classify the disturbances according to their underlying causes. Many previous studies on classification systems were reported, e.g., a neural network-based classification system was proposed in [4]. The study, however, does not classify the events according to their underlying causes which are drawing more interests than the types of events like sags or swells. In [5] an expert system was proposed to classify the seven underlying-causes based on voltage measurements. These underlying causes include: energizing, non-fault interruption, fault interruption, transformer saturation, induction motor starting, step change, and fault. In [6], the authors proposed a Support Vector Machine based classifier that focuses on voltage disturbances due to faults or transformer energizing. These studies emphasized that robust features play an essential role on the classification performance. Extracting effective features for all disturbances in large power systems is a very challenging task requiring good understanding from both power engineering and signal processing sides. In this study, the characterization of disturbances is further split into several groups of disturbances from different spatial zones of a grid-connected wind farm, and is described in detail in Section 4.

Fine location estimation

Once the underlying causes are known, the location of the source of disturbances is determined more accurately in the last stage based on voltage and current recordings obtained from the monitors in the coarsely estimated zone. This requires the underlying causes to be estimated in advance since different techniques are employed to estimate the source location for different types of disturbances. Some studies on tracking the source location of capacitor switching can be found in, e.g., [7] and [8]. In this study, we consider two types: fault and capacitive related switching (capacitor and cable switching). Our proposed method uses the information about the phase angles of the current before and during the disturbance to estimate the relative location of fault events. For capacitive related switching events, the relative location is estimated by comparing the initial phase angles of the fundamental and harmonic currents immediately after the inception instant of the disturbance. More details about the method are described in Section 5.

3 Coarse Location Estimation

Coarse location estimation is based on the detection parameter (DP) from the segmentation (See Appendix 7.2 for a brief review). The segmentation of the

voltage recordings uses the following detection parameter:

$$DP(n) = \left[\frac{1}{L_W} \sum_{n-L_W+1}^{n} (y(n) - \hat{y}(n)) \right]^2 \quad n = L_W, ..., L \tag{1}$$

The variance of residuals, i.e., the variance of the difference between the input and the reconstructed signals from the model, is used for detection, where a detection parameter is formed according to the accumulated energy of residuals over a short window of time [1]. Transition segments are detected from high values of the detection parameter. It is observed that the value of this detection function increases with the disturbance degree; the monitor closer to the disturbance location gives a higher value of the detection parameter. The monitor j that is closest to the origin of the disturbance can be estimated by selecting the maximum detection parameter value from the three phase recordings at different monitors:

$$DP(n) = \text{argmax}_j(\text{argmax}_k(DP_{j,k})) \tag{2}$$

where k=A, B, C are 3 phases; $j = 1, 2, ..., N$; N is the total number of monitors in the system. Care must be taken as voltages from different levels are different. Therefore, each voltage sequence is normalized by its normal operation value before employing (2), (i.e., value in pu). The proposed method is briefly described as follows:

- Normalize all voltage disturbance measurements to their normal operation voltage values in the corresponding voltage level.
- Apply Kalman filters to all normalized disturbance waveforms; compute the Kalman filter residuals and the detection parameters in (1).
- Find the maximum detection parameter during the transition segments according to (2).
- Normalize theses maximum detection parameters to the minimum one for convenient observation.
- The maximum detection parameter indicates the monitor closest to the location of the source of disturbances.

Detection parameter values selected from some monitors at different voltage levels for a three-phase fault at 130-kV cable terminal (close to the monitor m16, which is located in the substation on 130-kV side of the 400/130-kV transformer; see Appendix 7.1 for the single line diagram) are given in Table 1.

The highest values are found for the monitors m10 and m16. The coarse location estimation is in this case that the origin of the disturbance is in the 130-kV part of the system. The detection index is somewhat lower for the monitor m10

Table 1: Normalized detection parameters from different monitors for a three-phase fault.

	Phase A	Phase B	Phase C
Monitor m1 (20 kV)	4.1	3.4	3.4
Monitor m6 (20 kV)	4.2	3.5	3.5
Monitor m10 (130 kV)	5.8	4.9	4.6
Monitor m16 (130 kV)	**6.0**	**5.0**	**4.8**
Monitor m20 (400 kV)	1.6	1.8	1.0
Monitor m22 (400 kV)	1.6	1.8	1.0

than for the monitor m16, but this information is not used in the coarse location estimation.

Other examples for the unit tripping (unit 1 which is close to the monitor m1) and capacitor energizing (the capacitor bank on the transmission grid which is close to monitors m22 and m20) are shown in Table 2 and Table 3. The zones selected by the coarse location estimation are the feeder on the 20-kV grid where unit 1 is located and the 400-kV part of the system for the unit tripping and capacitor energizing events, respectively.

Table 2: Normalized detection parameters for a unit tripping.

	Phase A	Phase B	Phase C
Monitor m1 (20 kV)	**7.53**	**8.07**	**9.57**
Monitor m6 (20 kV)	7.52	8.07	9.56
Monitor m10 (130 kV)	3.13	1.42	1.59
Monitor m16 (130 kV)	2.84	1.31	1.49
Monitor m20 (400 kV)	2.19	1.0	1.15
Monitor m22 (400 kV)	2.18	1.0	1.15

Table 3 shows the results for a three-phase switching. Because the switching is applied at the zero crossing of phase A, the disturbance in phase A is much smaller than those in phases B and C. Thus, the detection parameter value for phase A is much smaller than those for phase B and C, and is easily being confused with a two-phase disturbance. We are, however, not using this information to identify which phases are involved in the disturbance but to confirm that the disturbance occurs in a zone on the 400-kV grid and close to the monitors m20 and m22.

Table 3: Normalized detection parameters for a capacitor energizing on the 400-kV grid.

	Phase A	Phase B	Phase C
Monitor m1 (20 kV)	1.00	32.08	24.17
Monitor m6 (20 kV)	1.00	31.38	23.70
Monitor m10 (130 kV)	1.03	48.75	46.09
Monitor m16 (130 kV)	1.00	48.89	46.87
Monitor m20 (400 kV)	2.25	497.24	427.36
Monitor m22 (400 kV)	**2.25**	**497.34**	**427.43**

4 Characterization and Classify Disturbances according to Underlying Causes

As mentioned earlier, for complex power systems, characterizing all possible types of disturbances is a challenging work and still requires a lot of further research and development. Once the approximate location of the source of disturbances (i.e., the coarse spatial zone) is estimated, the work becomes easier due to the smaller number of possible disturbances that may occur in a specific zone as compared to those in the whole system. This section tries to characterize some disturbances and aims at distinguishing some selected disturbances within the coarsely estimated zone. The analysis uses the measured currents and voltages obtained from the monitor associated with the highest detection parameter determined from Section 3.

4.1 Disturbances in a zone of 20-kV grid

Consider three disturbance classes on this grid: fault, unit switching, and capacitor energizing. Of these three classes, fault events are recognized in the preclassification as they contain more than one transition segment. The two remaining classes, consisting of only one transition segment, are further characterized by the following properties.

Unit switching

The monitor with the highest detection parameter in this case is the one connected to the terminal of the switched unit. An event is classified as unit-switching if:

- Voltage in the event segment is within the normal operating limit, and not rich in high-frequency components around the switching instant, as shown

in an example spectrogram in Figure 2.

- Absolute value of current change, ΔI as defined in (3), is high (e.g., > 0.9).

$$\Delta I = \frac{I_{event} - I_{pre-event}}{\max(I_{event}, I_{pre-event})} \tag{3}$$

where I_{event} and $I_{pre-event}$ are the currents before and during the event segment, respectively. The sign of I indicates a tripping or an energizing event.

Capacitor energizing

The monitor with the highest detection parameter in this case is the one that is closest to the capacitor. An event is classified as capacitor energizing if:

- Voltage in the event segment is within the normal operating limit, but rich in high-frequency components around the energizing point, as shown in the spectrogram in Figure 3.

4.2 Disturbances in a zone of 130-kV and 400-kV grids

Similar to the previous case, a fault event is distinguished by the number of transition segments. Consider the other two types of events on these grids: capacitor energizing and transformer energizing. Both capacitor and transformer energizing have harmonic contents at low frequencies. However, comparing their voltage spectrograms, capacitor energizing has relatively high energy at the high frequencies (above 500 Hz). Two examples are shown in Figure 4 and Figure 5.

5 Fine Location Estimation

Spatial information or information on the location of disturbances can be determined by several methods depending on the type of disturbances. In this section, relative locations (upstream, downstream) of fault events and capacitive related energizing events are considered.

The relative location of fault is determined by a simple rule based on comparing the phase angles of pre-fault and during-fault currents. Consider a simple system in Figure 6, assume that fault current is purely inductive and active power flow from A to B. Upstream and downstream are defined according to the direction of active power flow, i.e., a fault at F1 is an upstream fault and a fault at F2 is a downstream fault.

Consider the instant immediately after the fault inception instant and assume that:

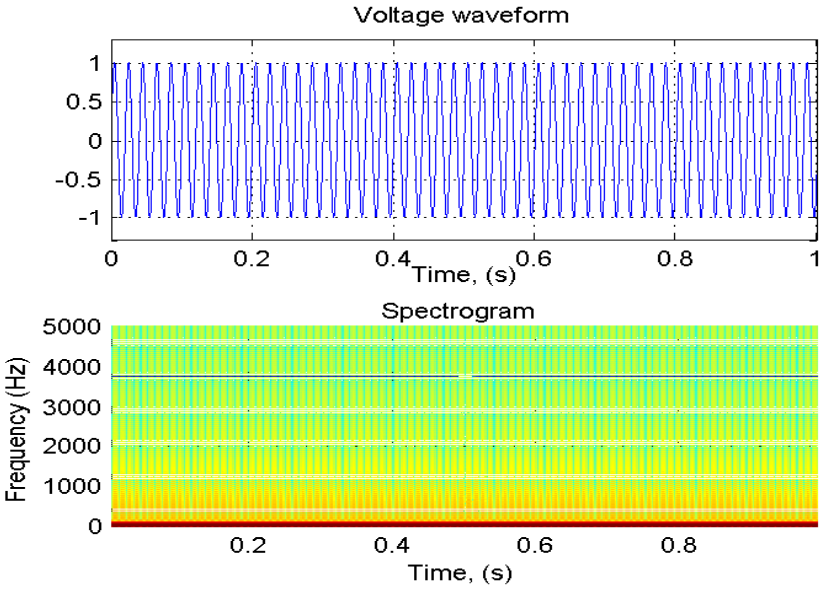

Figure 2: Unit tripping event (Unit 1 is tripped at 0.5 s).

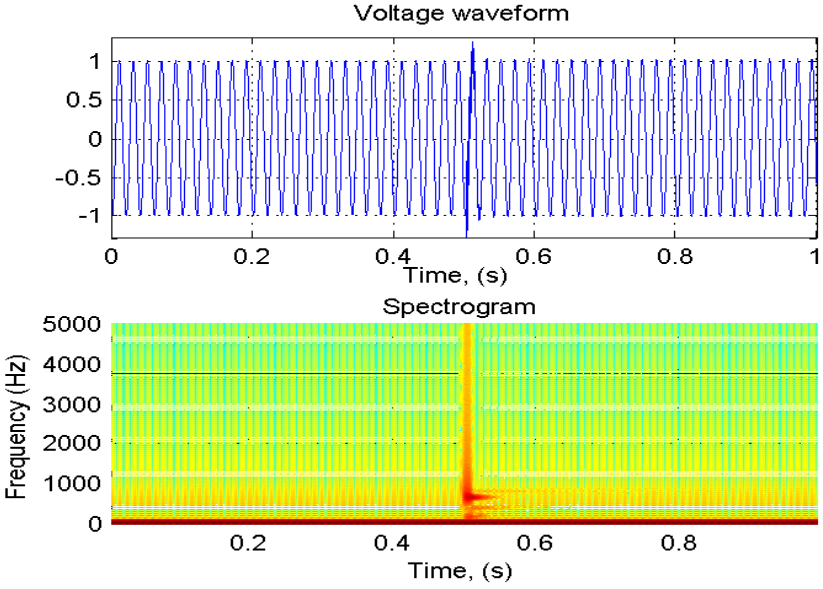

Figure 3: Capacitor energizing event (Capacitor is energized at 0.5 s).

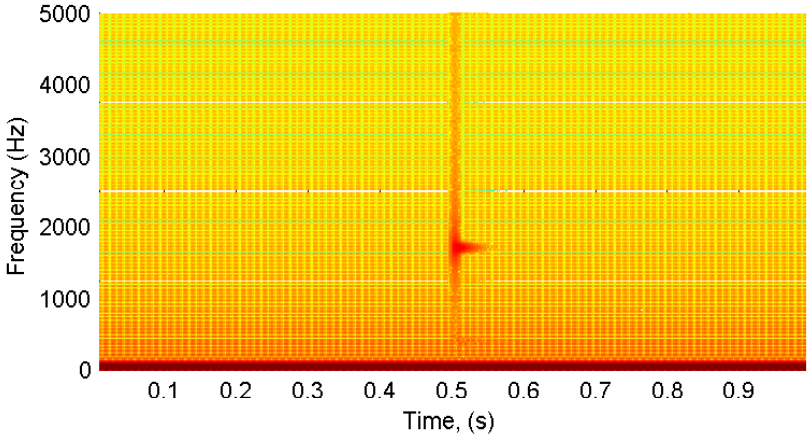

Figure 4: Voltage spectrogram of capacitor energizing.

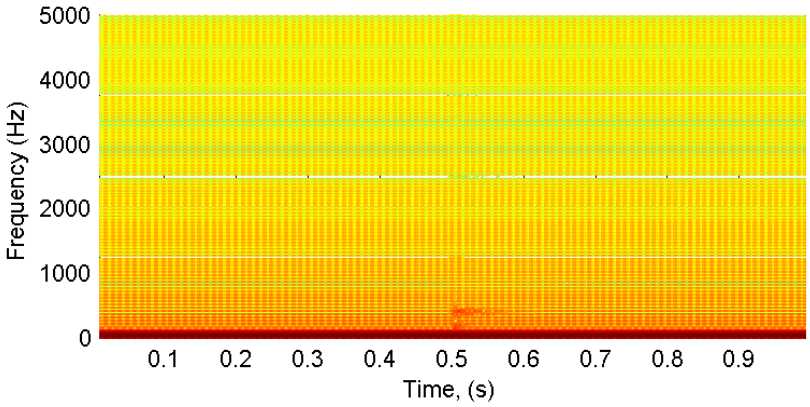

Figure 5: Voltage spectrogram of transformer energizing.

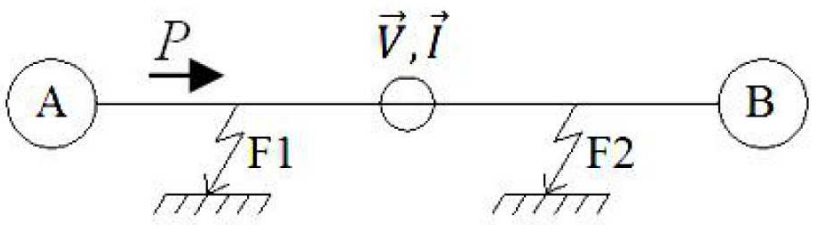

Figure 6: Simple system.

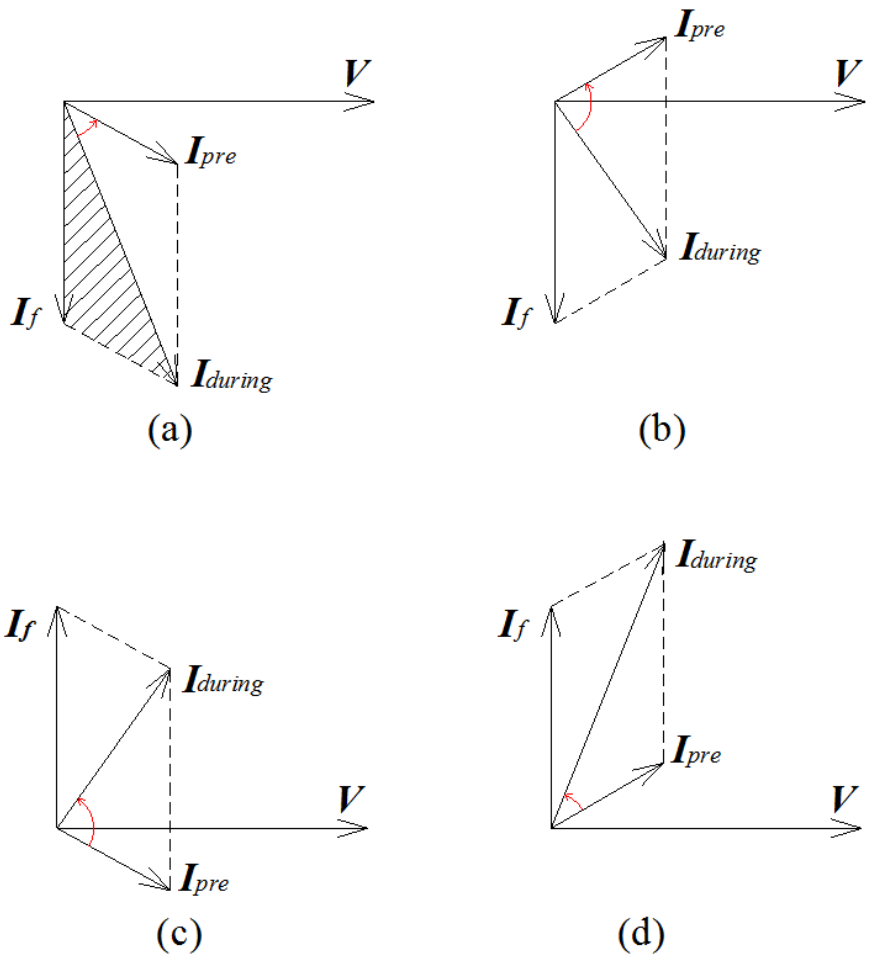

Figure 7: Phasor diagrams.

$$\boldsymbol{I}_{during} = \boldsymbol{I}_{pre} + \boldsymbol{I}_f \tag{4}$$

where $\boldsymbol{I}_{during}$ is the during-fault current, $\boldsymbol{I}_{pre}$ is the pre-fault or load current, $\boldsymbol{I}_f$ is the fault current. The pre-fault current may be either inductive or capacitive and the fault may occur either at F1 (upstream) or F2 (downstream). This leads to four possible combinations, as shown in Figure 7. By observing Figure 7(a) (inductive pre-fault current, downstream fault) and Figure 7(b) (capacitive pre-fault current, downstream fault), and assuming that the active power flow is from A to B, one can conclude that $\boldsymbol{I}_{pre}$ should lie somewhere in the positive plane of the real axis and the actual during-fault current should lie somewhere between $\boldsymbol{I}_f$ and $\boldsymbol{I}_{during}$ (the dashed region). Thus, in both cases of inductive or capacitive pre-fault current, $\boldsymbol{I}_{during}$ always lags $\boldsymbol{I}_{pre}$ as long as it is a downstream fault.

Similarly, for the cases of upstream fault, $\boldsymbol{I}_{during}$ always leads $\boldsymbol{I}_{pre}$. Figure 7(c)

and Figure 7(d) show the phasor diagrams of an upstream fault with inductive and capacitive pre-fault current, respectively. From this analysis, the relative fault location can be determined by comparing the phase angles of pre-fault and during fault currents. There are several algorithms developed to track the phase angles based on the zero crossings, FFT, and Phase Lock Loop. An example of a downstream fault by both zero crossings and FFT phase angle tracking (from EMTDC) is shown in Figure 8 which confirms the proposed method. The top plot in Figure 8 shows three zero-crossing points associated with a downstream fault.

"Before" and "After" denote the closest zero-crossings of fundamental current before and after the fault inception instant. "Estimated" denotes the estimated zero-crossing without presence of fault:

$$t_{estimated} = t_{before} + 0.5 * T \tag{5}$$

where T is the fundamental cycle. In this case, t_{after} is larger than $t_{estimated}$ implying that the during-fault current lags the pre-fault current. This confirms a downstream fault case. The bottom plot in Figure 8 shows the difference between the pre-fault and during-fault current angles computed by FFT in EMTDC. The negative value implies that the during-fault phase angle is smaller than the pre-fault phase angle or during-fault current lags the pre-fault current.

Location of fault events has been studied in many works. To the best of our knowledge, there are, however, not many similar studies for other events. Some studies on tracking the relative source location of shunt capacitor switching transients are presented, for example, in [7] and [8]. In this study, we observed that for capacitive energizing event family (capacitor or cable energizing); the relative location of disturbance source can be determined by looking at the initial direction of fundamental and harmonic currents. Based on the fact that, immediately after energizing instant, harmonic currents rush into the switched device, we can compare the initial phase angles of fundamental and harmonic currents to determine the relative switching location. The procedure is:

- Extract the fundamental (I_1) from the measured current (I).
- Calculate the total harmonic current: $I_h = I - I_1$
- Find the first peak in the harmonic current, denoted by the point: t_p on the time axis.
- Compare the direction of I_1 and I_h at the time instant t_p: If $I_1(t_p) * I_h(t_p) > 0$, the initial harmonic and fundamental currents are in the same direction, indicating a downstream energizing event, and the vice versa.

An example of an upstream energizing event and a downstream energizing event is given in Figure 9.

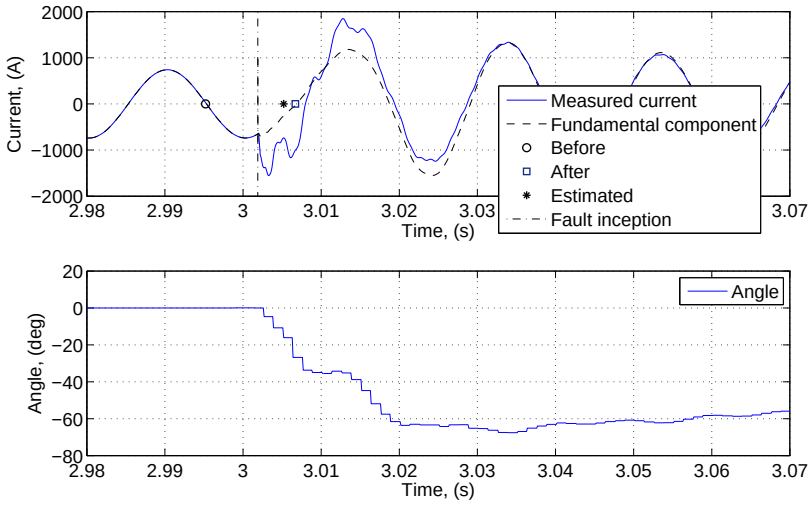

Figure 8: Phase angle tracking by zero crossing and FFT.

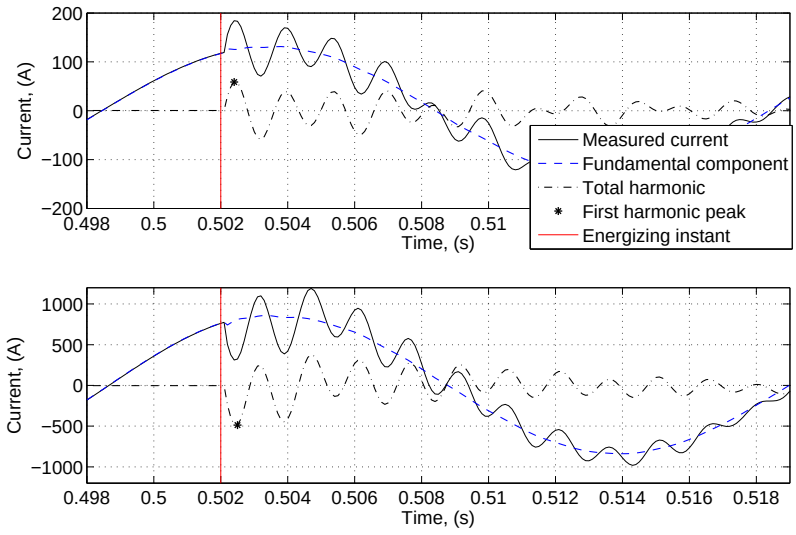

Figure 9: Capacitive energizing events. (Top: Downstream, Bottom: Upstream).

6 Conclusion

In this paper, we have presented a new method for estimating the origin of disturbances, and features for classifying the underlying causes of disturbances through event characterization, where disturbance data can be obtained from the power quality monitors in multiple levels and locations of a power system. Case studies to a grid-connected wind farm with focus on several selected disturbances were performed. It has been shown that the proposed method based on the maximum detection parameters resulted from the causal and anti-causal segmentation is reliable to identify the coarse spatial zone of the location of the source of disturbances. The study has also shown that by primarily identifying the location and classified disturbances based on the number of transition segments, it becomes easier to characterize and estimate the underlying causes of the remaining disturbances. Simple but efficient methods to determine the relative locations of disturbances by comparing the phase angles of fundamental and harmonic currents are presented. For the fault events, the relative location is determined by comparing the phase angles of the pre-fault and during-fault currents. A fault is downstream if during-fault current lags the pre-fault current, and conversely it holds for the upstream faults. Relative locations of capacitive energizing can be determined by comparing the initial phase angles of the fundamental and harmonic currents immediately after the energizing instant. If the initial harmonic and fundamental currents are in the same direction, is the event is classified as a downstream energizing event, and vice versa.

For developing a complete monitoring system, more studies are required, especially on disturbance characterization, or feature extraction and classification methods which are considered as part of our future work.

7 Appendix

7.1 The test system

The test system used for this study is a 255-MW wind park connected to a 400-kV transmission system via a 20-kV collector grid, transformers, and 130-kV cables. Each unit of wind turbine generator (WTG) consists of a 3-MW WTG and a 0.69/20-kV transformer as shown in Figure 10. Voltages and currents are measured at different measurement points indicated by the red circles. The system is simulated in EMTDC to generate data for this study.

7.2 The causal and anti-causal segmentation method

The segmentation method used for this paper has been described in detail in cite1. The aim of this section is to briefly review the method to give some basic understandings. The method uses the residuals from a Kalman filter under the harmonic

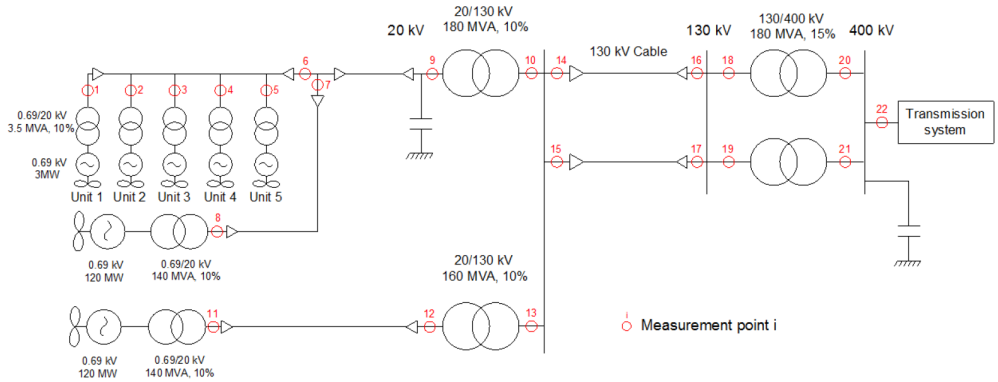

Figure 10: The test system.

model to detect abrupt changes in voltage measurements and is based on the segmentation method proposed in [9]. Under the harmonic model, a disturbance signal is modeled as the sum of M harmonics by:

$$y(n) = \sum_{m=1}^{M} s_m(n) + v(n) = \sum_{m=1}^{M} A_m e^{j\omega_m n} + v(n) \tag{6}$$

where $A_m = a_m e^{j\phi_m} = A_{m,r} + jA_{m,i}$ is the complex magnitude of the m^{th} harmonic; $A_{m,r}$ and $A_{m,i}$ are the real and imaginary parts; ϕ_m is the initial phase; ω_m is the frequency, and $s_m(n) = A_m e^{j\omega_m n}$ is the m^{th} harmonic signal component. The state and observation equations for scalar measurement data $y(n)$ are described in (7) and (8):

$$\begin{bmatrix} s_{1,r}(n) \\ s_{1,i}(n) \\ \vdots \\ s_{M,r}(n) \\ s_{M,i}(n) \end{bmatrix} = \mathbf{A} \begin{bmatrix} s_{1,r}(n-1) \\ s_{1,i}(n-1) \\ \vdots \\ s_{M,r}(n-1) \\ s_{M,i}(n-1) \end{bmatrix} + \frac{\omega(n)}{2M} \begin{bmatrix} 1 \\ 1 \\ \vdots \\ 1 \\ 1 \end{bmatrix} \tag{7}$$

$$y(n) = [1\ 0\ \ldots\ 1\ 0] \begin{bmatrix} s_{1,r}(n) \\ s_{1,i}(n) \\ \vdots \\ s_{M,r}(n) \\ s_{M,i}(n) \end{bmatrix} + v(n) \tag{8}$$

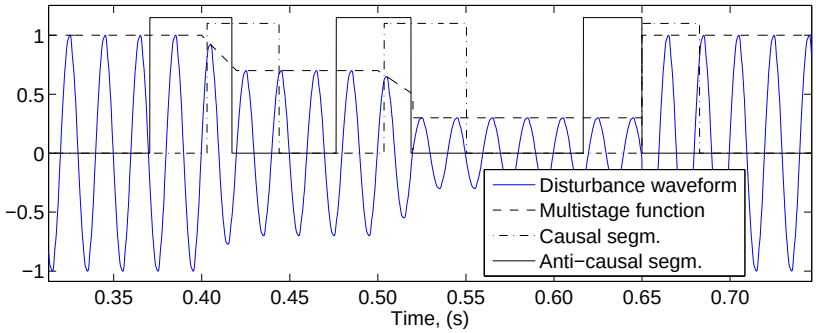

Figure 11: Segmentation result for multistage transition.

where

$$\mathbf{A} = \begin{bmatrix} \cos\omega_1 & -\sin\omega_1 & 0 & \dots & 0 & 0 & 0 \\ \sin\omega_1 & \cos\omega_1 & 0 & \dots & 0 & 0 & 0 \\ \vdots & \vdots & \vdots & \ddots & \vdots & \vdots & \vdots \\ 0 & 0 & 0 & \dots & 0 & \cos\omega_M & -\sin\omega_M \\ 0 & 0 & 0 & \dots & 0 & \sin\omega_M & \cos\omega_M \end{bmatrix} \tag{9}$$

The variance of residuals (or, the difference between $y(n)$ and the reconstructed signal from the model) is used for detection, where a Detection Parameter (DP) is formed according to the accumulated energy of residuals over a short window of time by:

$$DP(n) = \left[\frac{1}{L_W} \sum_{n-L_W+1}^{n} (y(n) - \hat{y}(n)) \right]^2 \quad n = L_W, ..., L \tag{10}$$

where $\hat{y}(n)$ is the reconstructed of $y(n)$; L_W is the analysis window length; L is the length of $y(n)$.

The analyzed signal is passed through this Kalman filter in both causal and anti-causal time directions. A change is detected if detection parameter exceeds a threshold. The study has shown that combination of causal and anti-causal segmentations gives accurate information about the transitions in voltage measurements. An example with multistage transitions is shown in Figure 11. In this example, a voltage measurement is multiplied with a multistage function and then segmented. The result shows that causal segmentation tends to introduce some detection delay and prolong the transition segment.

Combination of causal and anti-causal gives much more accurate transition segments. It is also worth noticing that slow transition is indicated by the existence of an overlap between the causal and anti-causal segmentations and fast transition is indicated by a gap. And for fast transitions, triggering point can be estimated by:

$$T = (T_{causal} + T_{anti-causal})/2 \tag{11}$$

where T_{causal} and $T_{anti-causal}$ are the starting time instants of causal and anti-causal transition segments.

References

[1] C. D. Le, I. Y. H. Gu, and M. H. J. Bollen, "Joint causal and anti-causal segmentation and location of transitions in power disturbances," *IEEE PES General Meeting*, Minneapolis, Minnesota, USA, July 25-29, 2010.

[2] A. Ukil and R. Živanović, "Automatic Signal Segmentation based on Abrupt Change Detection for Power Systems Applications," *IEEE Power India Conference*, 2006.

[3] S. Santoso, E. J. Powers, et al., "Power quality assessment via wavelet transform analysis," *Power Delivery, IEEE Transactions on*, vol. 11, no. 2, pp. 924-930, 1996.

[4] M. B. I. Reaz, F. Choong, et al., "Expert system for power quality disturbance classifier," *Power Delivery, IEEE Transactions on*, vol. 22, no. 3, pp. 1979-1988, 2007.

[5] E. Styvaktakis, M. H. J. Bollen, and I. Y. H. Gu, "Automatic classification of power system events using rms voltage measurements," *IEEE Power Engineering Society Summer Meeting*, 2002.

[6] P. G. V. Axelberg, I. Y. H. Gu, and M. H. J. Bollen, "Support vector machine for classification of voltage disturbances," *Power Delivery, IEEE Transactions on*, vol. 22, no. 3, pp. 1297-1303, 2007.

[7] S. Santoso, J. D. Lamoree, and M. F. McGranaghan, "Signature analysis to track capacitor switching performance," *Transmission and Distribution Conference and Exposition, IEEE/PES*, Atlanta, GA, USA, 28 Oct. - 02 Nov, 2001.

[8] G. W. Chang, J. P. Chao, et al., "On tracking the source location of voltage sags and utility shunt capacitor switching transients," *Power Delivery, IEEE Transactions on*, vol. 23, no. 4, pp. 2124-2131, 2008.

[9] E. Styvaktakis, *Automating power quality analysis*, PhD Thesis, Chalmers University of Technology, 2002.

Paper B

A New Accurate Segmentation Scheme for Power-System Disturbance Recordings

Cuong D. Le, Irene Y. H. Gu, and Math H. J. Bollen

Submitted to *IEEE Transactions on Instrumentation and Measurement*

The layout has been revised.

Abstract

This paper addresses two issues associated with segmentation of disturbance recordings: the first is to automatically estimate the accurate boundary of the transition segments; the second is to select the optimal threshold for the detection of a transition segment. A new segmentation scheme is proposed that jointly uses the causal and anti-causal approaches. This allows very accurate location in time of the underlying transition in the power system. Next, a novel automatic threshold setting approach is also proposed for the detection index used for the detection of transition segments. Using the proposed segmentation scheme and the statistically-based threshold setting, case studies are conducted for the Kalman filter-based segmentation method. It is shown that transition segments, especially the trigger points, are more accurately located as compared to conventional schemes. Tests are performed on semi-synthetic disturbance sequences as well as real disturbance sequences obtained from two different power networks. The results show that the proposed scheme is able to locate fast transitions with very high accuracy and to provide very good performance under different scenarios of depth of transition, speed of transition, and noise level.

Keywords: Power-system measurements, causal and anti-causal filter, power quality, segmentation, signal-processing applications, threshold selection.

1 Introduction

Power-system measurements have become much easier in recent years. Different types of equipment are permanently available to record voltages and currents. To make use of the resulting large amount of data, automatic analysis methods are needed. An important subset of the available data are so-called voltage and current events; power-system disturbances associated with changes in the power system, either in the grid, at production side or with the load. Power quality is one of the possible applications of such disturbances; the general supervision of the system becomes possible by automatic analysis of the disturbances. Before event analysis is applied it is necessary to accurately divide each disturbance sequence into transition segments and event segments, where different methodologies of analysis could be applied.

According to [1], there are three basic approaches for detecting transition segments. These three approaches are based on: time-dependent waveform features, highpass or bandpass filters, and parametric models. Conventional detection methods based on time-dependent waveform features and the definition of voltage events in [2] are mentioned in some studies, for example, [3] and [4]. In the second approach, wavelet filter-based detection is used in [5]-[8]. A detection method using high order cumulants is proposed in [9]. The method uses a notch filter at fundamental frequency that eliminates the fundamental sinusoid. The third approach employs a model that estimates the signal from noisy measurements. The residuals from the model containing valuable information are used to detect the transitions [1]. Part of the related work can be found in [10] and [11] where damped sinusoidal model and Kalman filtering are used. After this work, some other detection methods are introduced. In [12], for example, a Kalman filter is applied to detect some rectangular voltage events including dips, swells, and short interruptions. The study in [12] does not provide a complete evaluation of detection delays in different conditions but one case shows that for a dip to 0.7 pu starting at zero-crossing, the delay is 2.4 ms. Each method has its own advantages and disadvantages, although the final aim is the same, i.e., the segmentation must be able to detect and accurately locate in time transitions in voltage and current waveforms. These transition segments are in turn associated with the underlying transition in the power system, for example the opening of a switch or the initiation of a short-circuit fault.

The contributions of this paper are twofold. The first contribution is a novel causal and anti-causal segmentation scheme that locates the underlying power-system transitions with very high time accuracy. The causal-anti-causal segmentation scheme is then tested using real measurements to show its practical applications. The second contribution is a statistically-based approach to determine the optimal threshold for the detection index, rather than using a hard threshold value as for example in [11]. Selection of this threshold value may impact the accuracy of the location of transition segments and the false alarm rate of the detection of

transition segments.

The remaining of the paper is organized as follows. Section 2 reviews the basic principles of segmentation and the remaining problems to be solved. Section 3 describes the proposed causal and anti-causal segmentation scheme. The proposed threshold selection approach based on detection theory is presented in Section 4. Case studies for causal and anti-causal segmentation and for threshold setting are presented in Section 5 and Section 6, respectively. Some technical details of the Kalman filter-based causal and anti-causal segmentation method are discussed in Section 7. Section 8 presents some conclusions from the study.

2 Segmentation

The term segmentation has been widely used in many areas with the common meaning that it is a process of partitioning the object of interest into different parts (segments) in which each part has some specific properties that are distinct from the others. In speech processing, for example, segmentation is the process of identifying the boundaries between words, syllables, or phonemes in spoken natural languages [13]. With a similar definition, segmentation in power-system disturbance analysis is the process of identifying the boundaries between event (stationary) and transition (non-stationary) segments. In the power engineering literature, some other related terminologies are used, of which "triggering" and "event detection" are the most common ones. There are, however, some slight differences among the terminologies. While triggering or detection refers to the process of identifying the occurrence of an event without concern about the accurate time location of the event, segmentation is more strongly related with identifying the boundaries (i.e., the starting and ending points of event).

There are many automatic segmentation/detection methods introduced in the literature, as discussed in 1. Most of the methods use a so-called *"detection index"*, and the detection of a transition is performed by applying a fixed threshold to the detection index. However, it is not straight forward to determine such a threshold as it is a tradeoff between the detection rate and accuracy as well as the false alarm rate, and is also dependent on the measurement conditions.

A very interesting point observed from the conventional detection/segmentation methods is that the the time location of a fast underlying transition in the power system is not part of the transition segment, as shown in Figure 1. Due to the delay (caused by, for example, applying filter or other processing), the starting point of the transition segment is detected somewhat after the underlying transition.

3 Causal and Anti-causal Segmentation

In this section, we propose a new segmentation scheme namely *joint causal and anti-causal (CaC) segmentation*. It is observed in Section 2 that the conventional

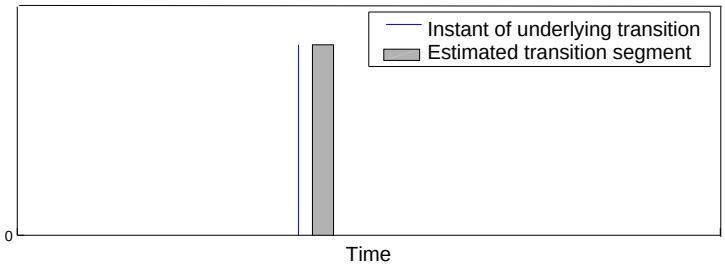

Figure 1: Example of conventional segmentation: detected transition segment lagging the occurrence instant of the underlying transition.

segmentation implemented in the *forward* (or, *causal*) time direction does not give an accurate time estimation of the underlying transition but instead a delayed transition segment. To solve this problem, the basic idea is to combine a causal analysis window with an anti-causal analysis window. It is worth mentioning that this joint scheme may be applied to any type of segmentation method using either time-dependent waveform features, highpass/bandpass filters, or parametric models. Based on the results from the two analysis windows, an accurate time allocation of the underlying transition is then obtained.

Assume that a transition from one state to another state takes place in a time duration of D_0 as represented by a transition of a voltage signal in Figure 2(a). The aim of the CaC segmentation is to allocate this duration.

In Figure 2(b), the *causal detection index* (for example, *di* in (8) in the appendix) increases gradually when the transition starts. When the causal detection index exceeds the threshold (the horizontal dashed line), a causal indication flag (the solid square wave) is triggered. This causal flag is reset when the causal detection index drops below the threshold. A similar process takes place in the opposite time direction (i.e., *backward* or *anti-causal*) and an anti-causal flag is obtained. Combining these two causal and anti-causal flags (the overlap between them) results in the final estimate of the underlying transition:

$$\hat{D}_0 = [T_{causal}, T_{anti-causal}] \tag{1}$$

where T_{causal} and $T_{anti-causal}$ are the trigger time instants of the causal and anti-causal flags. The shorter the duration of the underlying transition, the shorter the overlap between the two flags.

When the duration of the underlying transition decreases towards a single time instant T_0 (i.e., from a slow towards a fast transition), the overlap between the two flags no longer exists. There is, instead, a gap between them as shown in Figure 3(b). The middle point of this gap is used as an estimate of the instant of the underlying transition, T_0:

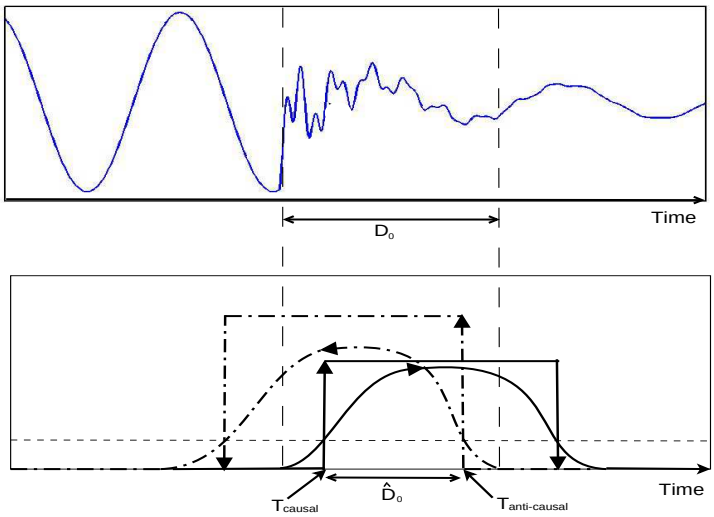

Figure 2: Illustration of CaC segmentation for a slow transition. From top to bottom: (a) A voltage waveform sequence containing a slow transition; (b) The detected transition flags by the causal method (solid line) and the anti-causal method (dashed line).

$$\hat{T}_0 = \frac{T_{causal} + T_{anti-causal}}{2} \tag{2}$$

The CaC segmentation algorithm is summarized as:

- If $T_{causal} < T_{anti-causal}$, then the transition is considered as slow. The estimated duration of the underlying transition is the duration of this overlap, $\hat{D}_0$, defined by (1).
- If $T_{causal} > T_{anti-causal}$, then the transition is considered as fast. There is a gap between the causal and anti-causal flags. The time location of the underlying transition is estimated as the middle point of this gap, $\hat{T}_0$, defined by (2).

4 Threshold Setting Based on Detection Theory

In this section, we propose a statistical method to automatically determine the threshold for the detection index, rather than using an empirically determined threshold value as for example in [11]. The method is based on the detection theory [14] and aim at setting a single threshold for detecting any type of event that may occur at the monitor location under a given false alarm constraint.

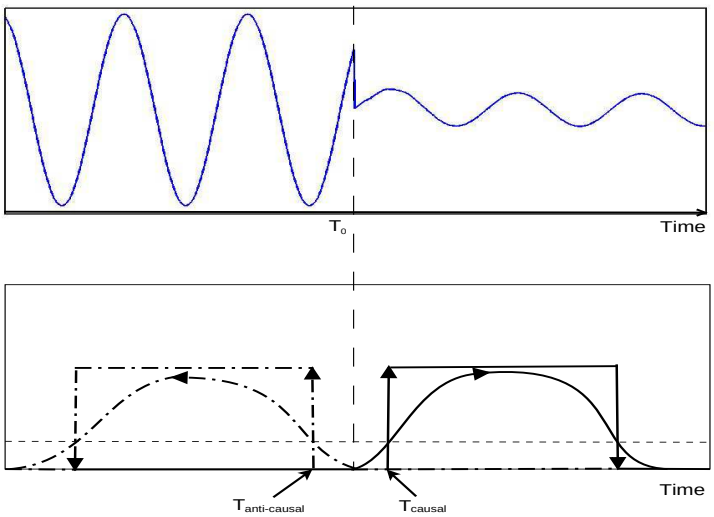

Figure 3: Illustration of CaC segmentation for a fast transition. From top to bottom: (a) A voltage waveform sequence containing a fast transition; (b) (b) The detected transition flags by the causal method (solid line) and the anti-causal method (dashed line).

During normal operation, the value of detection index *di* is small. If an event occurs in the power system, the model no longer fits the measurement which leads to an increase in *di*. Different types of event cause different increases of *di* during the transition segment. Figure 4 shows an example of detection index for two types of event.

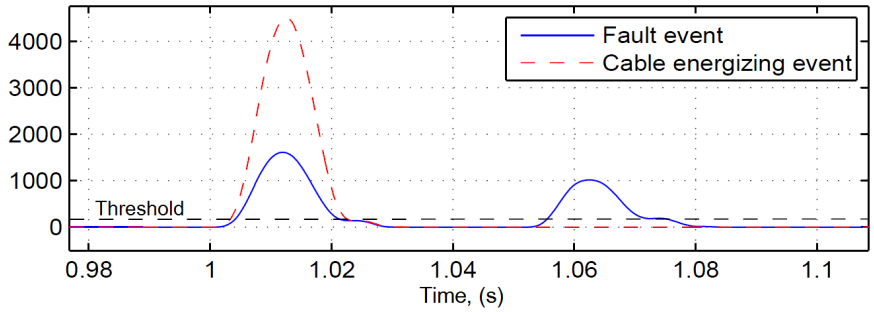

Figure 4: Example of detection index for two types of event.

The following relations are found between the threshold for the detection index and the performance of the segmentation is:

- Lower threshold → higher *false alarm rate*

- Higher threshold → longer *detection delay* and higher *miss* rate (*Miss* appears when the threshold is set too high.)

The aim of threshold setting is to find the optimal threshold that solve the conventional tradeoff between *false alarm* rate and *miss* rate. This optimal threshold can be determined by using the *Neyman-Pearsson* criterion [14] that maximizes the probability of detection under the probability of *false alarm rate* constraint. Let di_0 and di_1 be the corresponding detection indices for the normal operation segments and the transition segments, respectively. Let the two hypotheses be:

$$\begin{cases} \bullet\ \mathcal{H}_0(\textit{null hypothesis}) : di = di_0, di_0 \sim p(di \mid \mathcal{H}_0) \\ \quad \text{(is not a transition segment)} \\ \\ \bullet\ \mathcal{H}_1(\textit{alternative hypothesis}) : di = di_1, di_1 \sim p(di \mid \mathcal{H}_1) \\ \quad \text{(is a transition segment)} \end{cases}$$

where $p(di \mid \mathcal{H}_0)$ and $p(di \mid \mathcal{H}_1)$ are the probability density functions of di under *null hypothesis* and *alternative hypothesis*, respectively. And define the following probabilities:

- $P(\alpha_i; \mathcal{H}_j)$: probability of deciding α_i corresponding to hypothesis $\mathcal{H}_i$ when hypothesis $\mathcal{H}_j$ is true.
- $P_{FA} = P(\alpha_1; \mathcal{H}_0)$: *Type I error* probability, or probability of *false alarm*.
- $P_M = P(\alpha_0; \mathcal{H}_1)$: *Type II error* probability, or probability of *miss*.
- $P_D = P(\alpha_1; \mathcal{H}_1) = 1 - P_M$: probability of *detection*.

In order to find the optimal threshold, we have to estimate the probability density function (pdf) of di during the normal operation segments ($p(di \mid \mathcal{H}_0)$) and the pdf of di during the transition segments ($p(di \mid \mathcal{H}_1)$) as illustrated in Figure 5 and apply the *Neyman-Pearson* approach.

The *Neyman-Pearson* approach maximizes the probability of *detection* (P_D) for a given constraint on the maximum *false alarm* $P_{FA} = \alpha$. The decision is α_1 if:

$$L(di) = \frac{p(di \mid \mathcal{H}_1)}{p(di \mid \mathcal{H}_0)} > \gamma \tag{3}$$

where $L(di)$ is known as the *likelihood ratio* and the *threshold* γ is found from:

$$P_{FA} = \int_{\{di: L(di) > \gamma\}} p(di \mid \mathcal{H}_0) \mathrm{d}(di) = \alpha \tag{4}$$

Based on this approach, given the pdfs $p(di \mid \mathcal{H}_0)$, $p(di \mid \mathcal{H}_1)$, and the *false alarm* constraint α, the *threshold* γ for the detection index di can be determined.

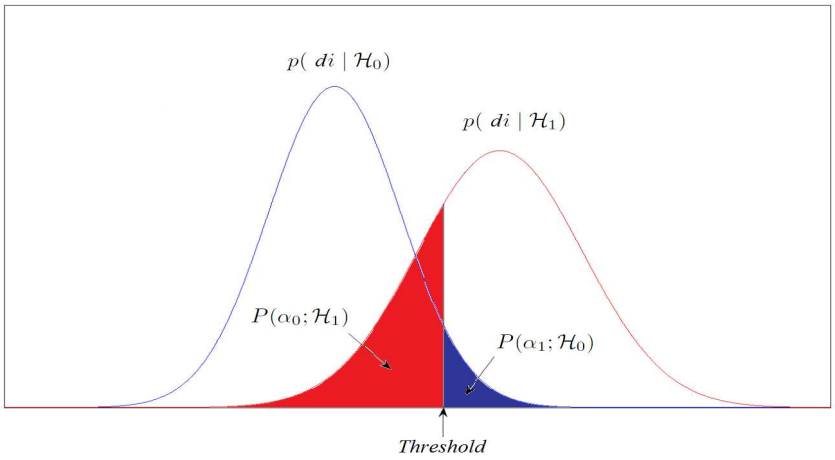

Figure 5: pdfs for two hypotheses.

5 Case Study: Causal and Anti-Causal Segmentation

The proposed causal and anti-causal segmentation scheme is tested on semi-synthetic data sequences where some preliminary tests are presented in our early work [15] and measured disturbances. In this section, examples of segmentation from the proposed scheme on one semi-synthetic sequence and two real disturbance recordings are included.

In the first case, a semi-synthetic disturbance waveform is obtained by multiplying a voltage recording with a multistage step/ramp function (an example is shown in the dashed line in Figure 6). The CaC segmentation is applied to this semi-synthetic disturbance and the results are shown in Figure 6(b) where the multistage step/ramp function (the dashed line) represents the underlying transition. From this result, one can see that the CaC segmentation shows very good performance, in terms of closely following the ground truth. The first two slow transitions are indicated by two segments and the third fast transition is indicated by an impulse as shown in Figure 6(b).

In the second case, the method is applied to a three-phase disturbance recording obtained at a 130-kV substation. Results of causal and anti-causal transition are shown in Figure 7.

From these segmentation results and the expert system rules presented in [16], it is concluded that:

• Since there is an overlap between the causal and anti-causal flags during the first transition in phases A and C, this is a slow transition and it indicates a fault inception between the two phases. The causal (and anti-causal) flag triggers at 61 ms (and 62 ms) and 62 ms (and 65 ms) for phase A and phase C, respectively. Phase B is not involved in the fault but there is some disturbance where the causal

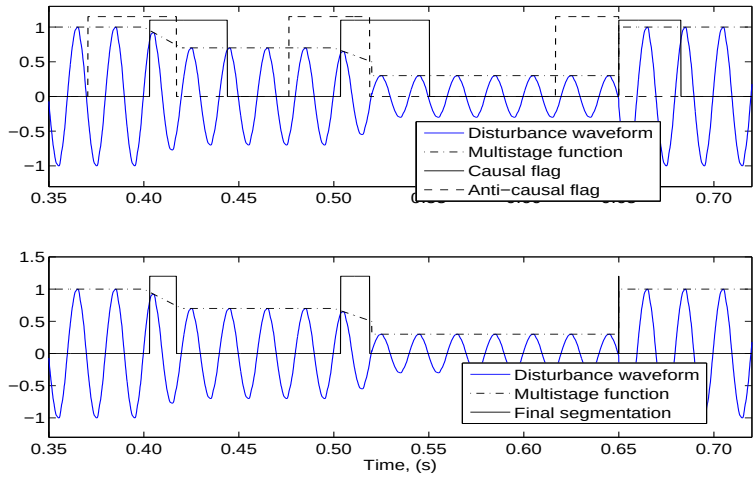

Figure 6: Segmentation for a semi-synthetic disturbance with multistage transition. From top to bottom: (a) Disturbance waveform with causal and anti-causal flags. (b) Disturbance waveform with final segmentation result.

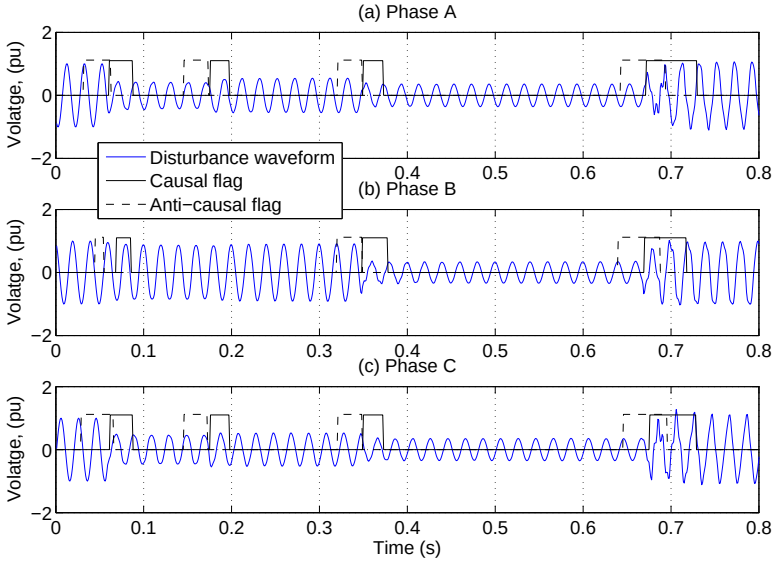

Figure 7: Segmentation for a real three-phase disturbance recording at 130 kV.

(and anti-causal) flag triggers at 70 ms (and 54 ms). Using (2), the estimated middle point of the gap between the two flags in phase B is at 62 ms. This implies that the underlying transition (fault inception) likely occurs at 62 ms. Note that what is a "slow transition" in phases A and C appears as a "fast transition" in phase B. The distinction between the fast and slow transitions obviously depends on the size of the change in voltage magnitude.

• The second fast transition, estimated to take place at 174 ms, indicates that there is a fast tripping of a line feeding the fault, which leads to a partial voltage recovery. This transition is so small that it cannot be detected in phase B.

• The third fast transition, estimated to take place at 349 ms, indicates that phase B gets involved in the fault.

• The last transition is a slow transition, estimated to take place at 672 ms, 670 ms, and 676 ms and end at 693 ms, 687 ms, and 695 ms for phases A, B, and C, respectively. The values of starting time and ending time are slightly different for the three phases but they all consistently show a slow voltage recovery in about 1 cycle followed by fault clearing. This time difference is likely due to the difference in circuit-breaker opening instants for the three phases [17].

The third case is a disturbance recording obtained from a transmission system [18]. By choosing a proper threshold for the detection index, the method shows very good performance on complicated events with multiple transition segments which can be observed in Figure 8 (Causal and anti-causal flags are removed for better observation, only the final segmentation results are presented).

Most of the transitions are detected in all three phases. There is, however, something missing at around 1.8 s observed from visual inspection. Visual observations show that that some transition occurs at this point but it is too small to automatically detect with the combination of detection function and threshold setting used. Improvement for automatic analysis of disturbance recordings needs to use a combination of detection functions.

6 Case Study: Threshold Setting

In this section, the proposed detection-theory-based threshold setting approach is studied. In order to find $p(di \mid \mathcal{H}_0)$ (defined in Section 4), twenty voltage measurements without transitions at the monitor location are used. These measurements are fed into the Kalman filter-based segmentation to compute the residual sequences and the detection index di (summarized in Section 9). In a similar way, $p(di \mid \mathcal{H}_1)$ is calculated by feeding the segmentation with a set of twenty semi-synthetic disturbance sequences obtained by multiplying a step function with twenty voltage measurements. Since the detection decision is based on the values of di in the computing window, $p(di \mid \mathcal{H}_1)$ and $p(di \mid \mathcal{H}_1)$ are calculated for the data in the sliding window before and after the triggering point of the transition. To demonstrate this, Figure 9 shows the semi-synthetic disturbance sequence and the time slots of two analysis windows applied to the detection index. The esti-

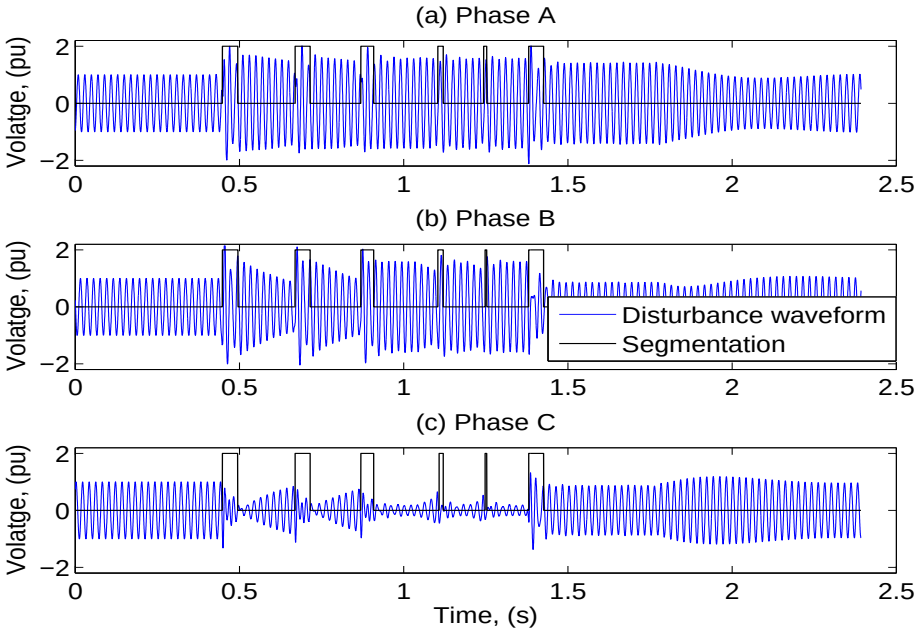

Figure 8: Segmentation for a three-phase disturbance recording obtained from Stattnet [18], 132-kV level. Causal and anti-causal flags are removed in this figure for better observations, only the final segmentation results are included.

mates of $p(di \mid \mathcal{H}_0)$ and $p(di \mid \mathcal{H}_1)$ in the two windows are given in Figure 10 where the mean values of detection index are 0.016 and 18.055, respectively.

The maximum value of di during normal operation observed for twenty measurements is denoted as the *critical detection index* ($di_{critical}$). Considering the most simple case where the threshold is set slightly above $di_{critical}$, i.e., the case where the false alarm rate is zero but detection delay is maximum. In this case, if there are any events associated with a di value at the trigger point smaller than $di_{critical}$, the segmentation needs to wait until di reaches this critical value to decide that an event is coming. This can lead to a *detection delay*.

In order to see how much the delay is, the threshold is set slightly above $di_{critical}$ and the segmentation is tested with another set of twenty semi-synthetic events obtained by the voltage measurements at the same monitor location, and the results are: There are 6 events detected with 1 sample (0.1 ms) delay, 9 events with 8 samples, 3 events with 9 samples, and 2 events with 10 samples as compare with the ground truths. The mean value of detection delays is 0.625 ms (1/32 cycle) which is rather small. From these results one can see that setting the threshold lower than $di_{critical}$ could reduce the delay time but increase the probability of false alarm. However, this is not necessary since the delay time is already very

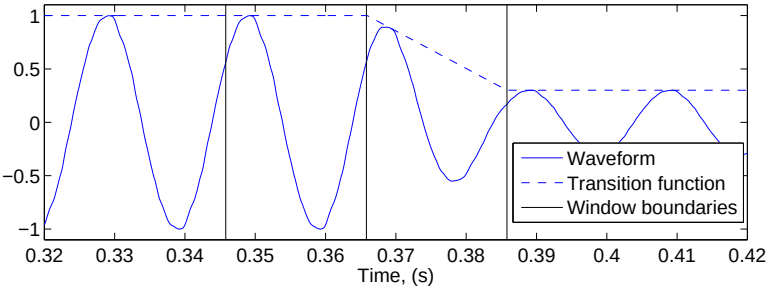

Figure 9: A semi-synthetic disturbance containing a slow transition with two windows: one before and one after the starting point of the transition.

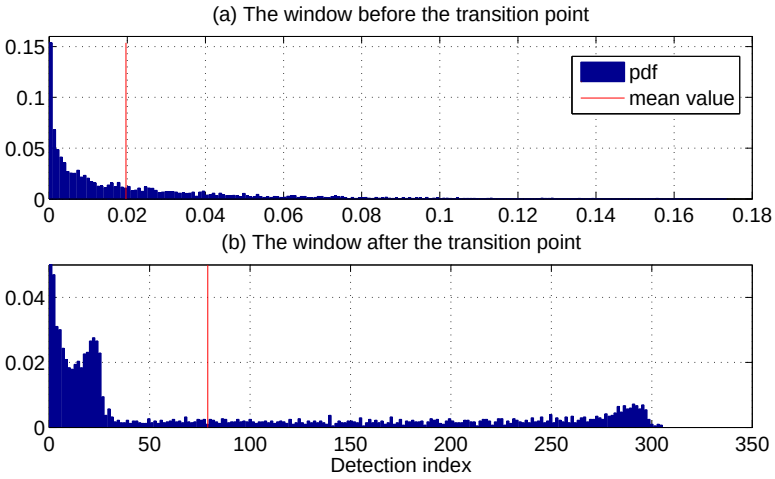

Figure 10: Estimated pdfs. From top to bottom: (a) $p(di \mid \mathcal{H}_0)$ estimated in the window before the starting point of the transition for 20 measurements; the mean value is 0.019. (b) $p(di \mid \mathcal{H}_1)$ estimated in the window after the starting point of the transition for 20 measurements; the mean value is 78.91. (Note the difference in the values of the detection index on horizontal axes.)

short. In addition, the detection delay only exists in this causal segmentation; using the joint causal and anti-causal segmentation, the time delay becomes even less critical.

7 Discussion

The proposed joint causal and anti-causal segmentation scheme is applied to a Kalman filter-based segmentation method. In this section, a number of technical issues about this segmentation method are further discussed.

7.1 On the selection of Kalman filter order

There is a tradeoff between computational burden and the accuracy of estimation. A higher order implies that more harmonics in the signal are modeled, and the remaining signal (considered as the model noise) is closer to white. However, if the aim is merely to detect the presence of an underlying transition, the accuracy of the signal estimation is of less interest than the change in the detection index around the time of the underlying transition. Figure 11 shows the values of the detection index for the same event (fault) but with two different values of Kalman filter order: $K = 5$ and $K = 15$.

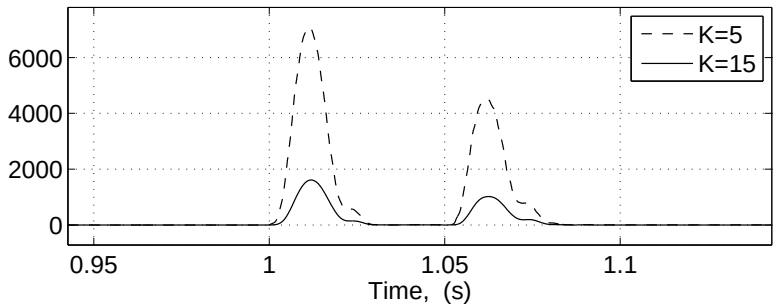

Figure 11: Detection index for the same event but with two different values of Kalman filter order.

From Figure 11 one can see that during the event segments, the detection index values obtained with $K = 5$ and $K = 15$ are almost the same since the signal is stationary and a high model order is not necessary to reduce the model unfit. On the other hand, during the two transition segments, there are more harmonics present in the signal, and a lower order causes higher model unfit, hence higher detection index. In the case of $K = 5$, the detection index jumps to a higher value after the trigger point, and this makes it easier for the decision of segmentation. A lower order filter is, however, not recommended for noisy signals as it impacts the robustness of the segmentation, hence leads to increased false alarm. Thus,

the selection of Kalman filter order depends on the application and the nature of the signal to be analyzed. In this study, an order of 15 has been selected.

7.2 On the selection of window length

Regarding the length of the sliding window used to calculate the detection index, there is a tradeoff between the time resolution and the smoothness of the detection index. When the window length decreases, the computed detection index increases faster after the trigger point as shown in Figure 12, hence it is possible to obtain a more accurate boundary of the transition segments.

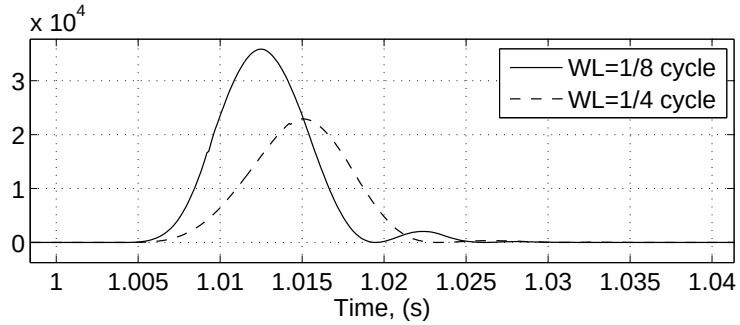

Figure 12: Detection index for the same event but with two different sliding window lengths (WL).

However, if the window length is too short, the detection index becomes less smooth and may contain several peaks within one transition segment. This makes it difficult to decide whether there is one or more than one transition segment. In this study, the window length is selected to be 1/4 cycle after considering these tradeoff issues.

7.3 On the performance of the method

Some preliminary performance evaluation of the proposed CaC Kalman filter-based segmentation method is discussed in [15]. In this section, the performance of the proposed scheme is further evaluated under different scenarios of point on wave, depth of transition, speed of transition, and noise level.

Impact of point on wave: A semi-synthetic disturbance sequence containing a fast transition from 1 pu to 0.7 pu is applied at different points on wave (i.e., at location with different phase angles). The evaluation shows that transitions close to zero crossings have lower maximum values of the detection index, are more difficult to detect and give longer delay time. There is less than one sample delay if the transition is applied at other points on wave. The values of delay around zero-crossings

are still rather small and the maximum delay is about 12 samples (1.2 ms).

Impact of depth of transition: For fast disturbances due to step changes, the impact of various sizes of the change in voltage magnitude (depths of transition) on the segmentation has been studied. Different sizes of voltage change at the upward zero crossing have been applied. The results show that a 0.01-pu step change is detected with 6.9-ms delay. There is less than one sample delay if the depth is greater than 0.4 pu. These values are obtained for the most-difficult-to-detect scenario (i.e., transition at zero crossing); for transitions at other points, the performance is better.

Impact of speed of transition: The evaluation performed in [15] shows that the detection delay decreases with the increase of transition speed: fast transitions are detected with less delay than slow transitions. It is shown that a very slow transition (0.3-pu step change in 3000 samples or 15 cycles) is detected with a delay of only 98 samples (around 0.5 cycle). This means that when using the causal and anti-causal scheme, fast transitions are estimated more accurately than slow transitions.

Impact of noise level: From the central limit theorem, combining independent noise sources leads to Gaussian distributed noise if the number of sources is sufficiently large. However, Gaussian distribution is not the case for the real power-system measurement noise. In practical cases one cannot treat the power-system measurement noise as white Gaussian. In our study, noise is obtained by passing the real measurements through a highpass filter. The obtained noise sequences are then scaled by a factor and added to the disturbance to obtain different noise levels.

In the first case, the segmentation is trained at a low noise level and tested at a higher noise level, without change of the threshold. In this case, the increase of noise level does not lead to increase of detection delay. In contrast, the delay is slightly reduced due to the fact that with increase of noise, residuals and its squared mean (the detection index) increase while the threshold is kept. Thus, the segmentation is more sensitive and the detection delay reduces, but there is an increase in *false alarm* rate. Test results show that with $SNR > 48$ dB, the segmentation works properly and there is no significant difference in delay time for both fast and slow transitions as compared to the case without additive noise. With $SNR < 48$ dB, the segmentation generates false alarms.

In the second case, the segmentation is re-trained and tested with the signal plus the additive measurement noise. The thresholds for different signal-to-noise (SNR) values are determined. The results show that the segmentation does not work properly with $SNR < 10$ dB. At $SNR = 10$ dB, the signal is very noisy and the segmentation works with a delay of 111 samples (0.56 cycle) and yields no false alarm as shown in Figure 13.

A case study is also conducted with different transition speeds. It is shown

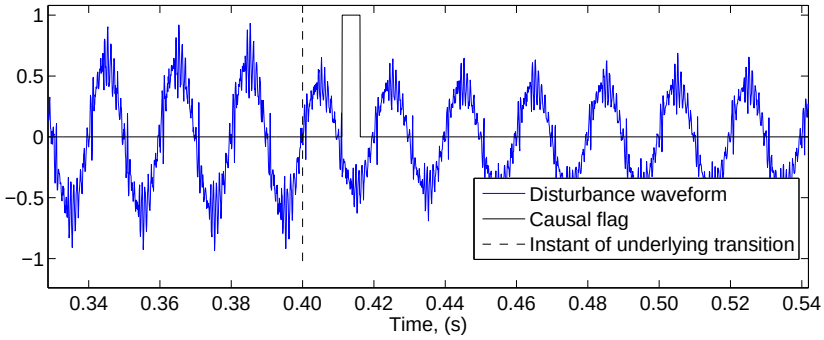

Figure 13: Segmentation for very noisy signal ($SNR = 10\,\mathrm{dB}$).

that by adapting the threshold to new noise, the segmentation is able to work properly with very high noise level. In this case, the detection delay is higher with higher noise level; the difference, however, is not significant. As the noise increases above a certain level, the segmentation can no longer detect slow transitions.

8 Conclusion

The proposed joint causal and anti-causal scheme and the statistically-based threshold setting approach have been applied for segmentation of power-system disturbance recordings. Results from theoretical analysis and experimental tests have shown that the proposed method is able to provide significantly improved segmentation results as compared with the conventional methods, in terms of providing more accurate estimation in time of the underlying transitions in the power system. For disturbances with fast transitions, the proposed segmentation scheme generates accurate estimations of the location of the underlying transition. For slow transitions, the underlying transition is accurately located in time. Further, using the proposed scheme, the duration of slow transition segment is shown to be slightly shorter than the duration of the underlying transition due to the detection delays in both directions. Fast and slow transitions are distinguished by whether there exists an overlap or a gap between the causal and anti-causal segmentation flags.

The proposed statistically-based threshold setting method has been tested for automatic setting the threshold for the detection index. The results show that by choosing an appropriate threshold, the segmentation may be without false alarms and with short detection delay. The threshold value is dependent on the measured noise, and is better trained using measurements at the monitoring point. By adapting the threshold to the measurement noise level, the segmentation is able to work with very noisy disturbances without false alarms and with no significant difference in detection delay. Our study also showed that the segmentation perfor-

mance is impacted by the point on wave, depth of transition, speed of transition, and noise level. These impacts are, however, not significant.

9 Appendix: Kalman Filtering and Detection Index

In this appendix, we briefly review the Kalman filter and the calculation of the detection index resulted from the Kalman filter residuals. Kalman filter uses state-space modeling to estimate the signal from noisy measurements [19]. Under the harmonic model, a disturbance signal is modeled as the sum of M harmonics in white noise by (5):

$$y(n) = \sum_{m=1}^{M} s_m(n) + v(n) = \sum_{m=1}^{M} A_m e^{j\omega_m n} + v(n) \tag{5}$$

The state and observation equations for scalar measurement data $y(n)$ are described in (6) and (7):

$$\begin{bmatrix} s_{1,r}(n) \\ s_{1,i}(n) \\ \vdots \\ s_{M,r}(n) \\ s_{M,i}(n) \end{bmatrix} = \mathbf{A} \begin{bmatrix} s_{1,r}(n-1) \\ s_{1,i}(n-1) \\ \vdots \\ s_{M,r}(n-1) \\ s_{M,i}(n-1) \end{bmatrix} + \frac{\omega(n)}{2M} \begin{bmatrix} 1 \\ 1 \\ \vdots \\ 1 \\ 1 \end{bmatrix} \tag{6}$$

$$y(n) = [1\ 0\ \ldots\ 1\ 0] \begin{bmatrix} s_{1,r}(n) \\ s_{1,i}(n) \\ \vdots \\ s_{M,r}(n) \\ s_{M,i}(n) \end{bmatrix} + v(n) \tag{7}$$

where

$$\mathbf{A} = \begin{bmatrix} \cos\omega_1 & -\sin\omega_1 & 0 & \ldots & 0 & 0 & 0 \\ \sin\omega_1 & \cos\omega_1 & 0 & \ldots & 0 & 0 & 0 \\ \vdots & \vdots & \vdots & \ddots & \vdots & \vdots & \vdots \\ 0 & 0 & 0 & \ldots & 0 & \cos\omega_M & -\sin\omega_M \\ 0 & 0 & 0 & \ldots & 0 & \sin\omega_M & \cos\omega_M \end{bmatrix}$$

and $\boldsymbol{A}_m = A_m e^{j\phi_m} = A_{m,r} + jA_{m,i}$ is the complex magnitude of the m^{th} harmonic; $A_{m,r}$ and $A_{m,i}$ are the real and imaginary parts; ϕ_m is the initial phase; ω_m is the frequency, $s_m(n) = A_m e^{j\omega_m n}$ is the m^{th} harmonic signal component, $v(n)$ is the measurement noise, and $\omega(n)$ is the modeling noise, assumed to be zero mean white.

The squared mean of the residuals in an analysis window (or, the squared mean of the difference between $y(n)$ and the reconstructed signal $\hat{y}(n)$ from the model) is used as a *detection index* (*di*) [11]:

$$di(n) = \left[\frac{1}{L_W} \sum_{n-L_W+1}^{n} (y(n) - \hat{y}(n)) \right]^2 \quad n = L_W, ..., L \tag{8}$$

where L_W is the analysis window length; L is the length of $y(n)$. Figure 14 shows an example of detecting transitions based on the residual sequence from a Kalman filter, where a detection window of 1/4 cycle (5 ms) is used.

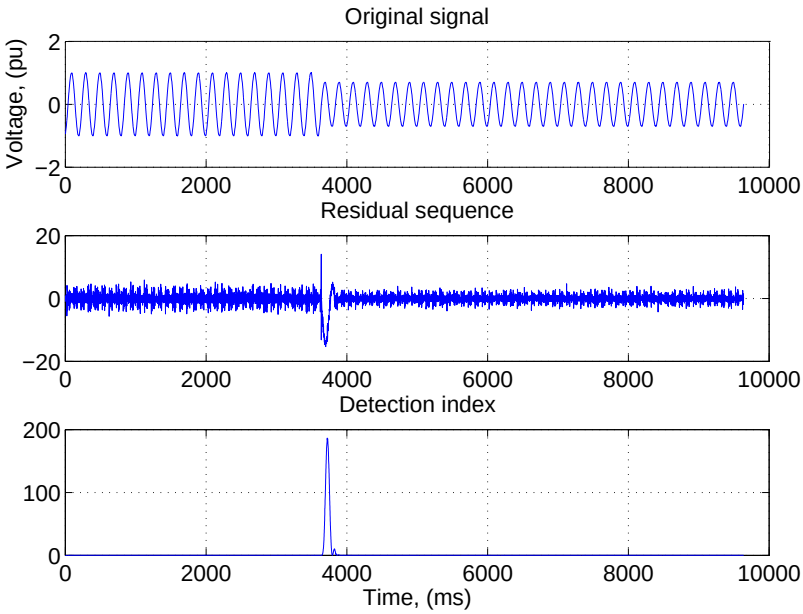

Figure 14: Example of detecting transition. From top to bottom: (a) Original voltage waveform; (b) Residual sequence from the Kalman filter; (c) Resulting detection index obtained from (8).

Acknowledgement

Thanks are due to Sarah Rönnberg and Mats Wahlberg from Luleå University of Technology for the measurement data used in the simulations.

References

[1] M. H. J. Bollen, I. Y. H. Gu, et al., "Bridging the gap between signal and power," *IEEE Signal Processing Magazine*, pp.12-31, Jul. 2009.

[2] M. H. J. Bollen, *Understanding power quality problems: Voltage sags and interruptions*, New York: IEEE Press, 1999.

[3] R. Naidoo and P. Pillay, "A new method of voltage sag and swell detection," *Power Delivery, IEEE Transactions on*, vol. 22, no. 2, pp. 1056-1063, 2007.

[4] T. Radil, P. M. Ramos, et al., "PQ monitoring system for real-time detection and classification of disturbances in a single-phase power system," *Instrumentation and Measurement, IEEE Transactions on*, vol. 57, no. 8, pp. 1725-1733, 2008.

[5] S. Santoso, E. J. Powers, and W. M. Grady, "Electric power quality disturbance detection using Wavelet transform analysis ", in *Proc. IEEE Int. Symp. Time-Frequency and Time Scale Anal.*, pp. 166-169, 1994.

[6] S. Santoso, E. J. Powers, et al., "Power quality assessment via Wavelet transform analysis," *Power Delivery, IEEE Transactions on*, vol. 11, no. 2, pp. 924-930, 1996.

[7] E. Pérez and J. Barros, "A proposal for on-line detection and classification of voltage events in power systems," *Power Delivery, IEEE Transactions on*, vol. 23, no. 4, pp. 2132-2138, 2008.

[8] A. M. Gaouda and M. M. A. Salama, "Monitoring nonstationary signals," *Power Delivery, IEEE Transactions on*, vol. 24, no. 3, pp. 1367-1376, 2009.

[9] O. N. Gerek and D. G. Ece, "Power-quality event analysis using higher order cumulants and quadratic classifiers," *Power Delivery, IEEE Transactions on*, vol. 21, no. 2, pp. 883-889, 2006.

[10] E. Styvaktakis, I. Y. H. Gu, and M. H. J. Bollen, "Voltage dip detection and power system transients," *Power Eng. Society Summer Meeting*, vol. 1, pp. 683-688, Jul., 2001.

[11] E. Styvaktakis, "Automating power quality analysis," PhD dissertation, Dept. Signal and Systems, Chalmers Univ. Technology, Sweden, 2002.

[12] J. Barros, and E. Pérez, "Automatic detection and analysis of voltage events in power systems," *Instrumentation and Measurement, IEEE Transactions on*, vol. 55, no. 5, pp. 1487-1493, 2006.

[13] E. Vidal and A. Marzal, "A review and new approaches for automatic segmentation of speech signals," in *Proc. European Signal Processing Conf., (EUSIPCO'90),* Barcelona, Spain, September, 1990, pp. 43-55.

[14] S. M. Kay, *Fundamentals of statistical signal processing - Detection theory*, Prentice-Hall PTR, 1998.

[15] C. D. Le, I. Y. H. Gu, and M. H. J. Bollen, "Joint causal and anti-causal segmentation and location of transitions in power disturbances," IEEE PES General Meeting, Minneapolis, Minnesota, USA, July 25-29, 2010.

[16] E. Styvaktakis, M. H. J. Bollen, and I. Y. H. Gu, "Expert system for classification and analysis of power system events," *Power Delivery,IEEE Transactions on*, vol. 17, no. 2, pp. 423-428, 2002.

[17] M. H. J. Bollen, "Voltage recovery after unbalanced and balanced voltage dips in three-phase systems," *Power Delivery, IEEE Transactions on*, vol. 18, no. 4, pp. 1376-1381, 2003.

[18] Stattnet data recordings, available online at: http://dfr.statnett.no/

[19] R. G. Brown and P. Y. C. Hwang, "Introduction to random signals and applied Kalman filtering with MATLAB exercises and solutions," John Wiley and Sons, New York, 1997.

Paper C

A Method to Evaluate Harmonic Model-Based Estimations under Non-White Measured Noise

Cuong D. Le, Math H. J. Bollen, and Irene Y. H. Gu

Preliminarily accepted, *IEEE PowerTech Conference,*
June 2011

The layout has been revised.

Abstract

Automatic extracting information from power-system event recordings requires applications of signal-processing estimation techniques whose performance has been verified under white noise. This paper proposes a method to test these techniques under real power-system noise, which is very different from white noise, to evaluate their application feasibility. The first part of the paper describes the evaluation method used to evaluate the techniques in a statistical sense and a method to extract noise from measured power-system recordings. The second part of the paper focuses on the evaluation of a number of harmonic model-based techniques under non-white noise, including: Kalman filter, MUSIC, ESPRIT, and segmentation algorithms. The paper shows that for the Kalman filter, a very high order with high computational burden is necessary only if high frequency components are of interest. The application of MUSIC, ESPRIT, and the segmentation algorithms under natural power-system noise is shown to be feasible.

Keywords: Harmonic analysis, performance evaluation, power quality, signal-processing applications.

1 Introduction

Signal-processing techniques are widely applied in power engineering, especially those related to the estimation of harmonics/interharmonics [1]-[2]. A number of currently used estimation techniques in power engineering employ a harmonic model under the assumption that the observation signal is a combination of different harmonics plus white noise [3]. However, measurements show that the spectrum of real noise is far from that of white noise, and this may impact the performance of the estimation. Some properties of power-system noise can be found in, e.g., [4]. Thus, it is desired to evaluate the performance of these techniques under real (measured) noise.

The main difficulty to evaluate the estimation techniques applied in power engineering is the lack of the *"ground truth"* signal to compare with. If synthetic data with white noise is used, the parameters of the signal are predefined which are the needed reference but the noise is not realistic. On the other hand, if the measurement data is used, the model is exposed to the real measurement noise (non-white) but there is no reference to compare with since the content of the measurement signal is unknown. A previous study [5] proposes a method to create semi-synthetic data sequences by embedding the measured noise into the synthetic data through superimposing real measurements with synthetic data. Such semi-synthetic data sequences are used in [5] to evaluate the performance of estimated frequencies and amplitudes of damped sinusoids from a frequency estimation method, ESPRIT (Estimation of Signal Parameters via Rotational Invariance Techniques) [6], which is able to detect and quantify harmonic and inter-harmonic components in a time-varying voltage or current signal [7].

In this study, we introduce a systematic method to evaluate the performance of harmonic model-based estimation techniques under real power-system noise. The first application of the proposed method is to find the model order small enough to have less computational burden but acceptable accuracy (i.e., trade-off between model order and computational demand). This is based on the observation that the higher the model order, the closer the noise spectrum moves towards white (as more harmonics are shifted from the noise subspace to the signal subspace), hence the more accurate the estimation becomes but the heavier the computational burden is. The second application is to evaluate the model-based estimation techniques where the observed noise deviates from the white noise assumption in the model, and to obtain statistic properties of their performance under different measured (color) noise levels and realizations. The method is applied but not limited to a number of estimation techniques under harmonic models, including Kalman filters, ESPRIT [6], MUSIC (Multiple Signal Classification) [8], and a segmentation algorithm [9]. The performance is evaluated using semi-synthetic data (i.e., synthetic signal plus measured power-system noise).

In the first case study, the impact of model order selection on the estimation accuracy of model-based techniques for harmonic estimation is studied as there is

a trade-off between the estimation accuracy and computational burden. To study the impact of the model order on the estimation accuracy, we evaluate the rms error of the Kalman filter applied to both clean and noisy signals. In the second case study, three estimation methods are evaluated under different signal-to-noise ratios (SNRs). Each method is evaluated using numerous realizations of semi-synthetic data sequences (i.e., different measured noise sequences are superimposed into a synthetic signal). The three methods studied are the Kalman filter-based event segmentation, the ESPRIT and MUSIC based harmonic estimation methods.

The remaining part of the paper is organized as follow: Section 2 briefly describes the evaluation method. The measurement noise extraction method is presented in Section 3, and the simulation results of the study are presented in Section 4. Conclusions and future work are drawn in Section 5.

2 The Evaluation Method

The evaluation method is a statistically-based method. A large number of measurements of voltage and/or current in the power systems are collected. In principle, the measurements should be done at the locations where the methods and applications are likely to be applied. Since the measured noise also contains the dominant fundamental voltage or current that is typically at least an order of magnitude larger than the true power-system background noise of interest, prefiltering is first applied to remove or suppress the fundamental. The result from the pre-filter to each measurement sequence is used as one noise realization.

Each noise realization is then added to a synthetic signal with predefined parameters to create the so-called semi-synthetic data that is used to evaluate the selected estimation techniques. The output of the estimation technique is compared with the predefined parameters of the synthetic input signal. The process is repeated for all noise realizations to obtain statistical properties for the performance of the selected estimation techniques. The estimated values are compared with the predefined parameters in the synthetic signal and a number of metrics for performance evaluations of the estimation technique are calculated. The performance metrics used in our study include mean values, rms errors, and standard deviation of the estimation error.

3 Noise Extraction

3.1 Signal and noise model

Under the harmonic model, a signal is modeled as the sum of K harmonics by (1).

$$y(n) = \sum_{m=1}^{M} s_m(n) + v(n) = \sum_{m=1}^{M} A_m e^{j\omega_m n} + v(n) \tag{1}$$

where $s_m(n)$ is the m^{th} harmonic component and $v(n)$ is the model noise assumed to be white. Under this model, apart from the K harmonics of interest, the remaining of the semi-synthetic signal $y(n)$ is considered as noise which means that the second and all higher order harmonics in the input signal are treated as noise if the model order is one. It is obvious that in measured power system data, the noise is not white as there always exist some harmonics. Thus, it is important to examine the impact of the model order as well as different noise levels and noise realizations.

3.2 Noise extraction

As described in Section 1, the step of noise extraction is aimed at maximally removing 50/60-Hz fundamental voltage/current in each measured noise sequence. An optimal linear-phase finite impulse response (FIR) filter using the Parks-McClellan algorithm ([10]) is used to remove the fundamental from the measurement data to obtain different realizations of noise sequences. Figure 1 and Figure 2 show an example of noise extraction, where the waveforms and FFT spectra before and after the noise extraction are included.

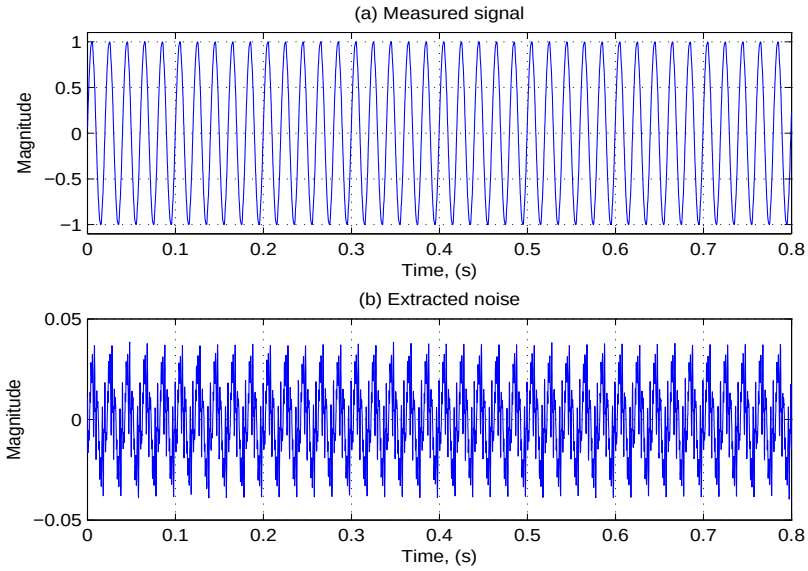

Figure 1: Waveforms of measured noise embedded in 50-Hz voltage (top) and the extracted noise (bottom). Note the difference in vertical scale.

From Figure 2 one can see that apart from the fundamental component (whose magnitude is unity but cut off for better display in Figure 2(a), there is no significant difference in the harmonic components of the measured signal and the extracted noise at frequencies above 200 Hz. However, the broadband components

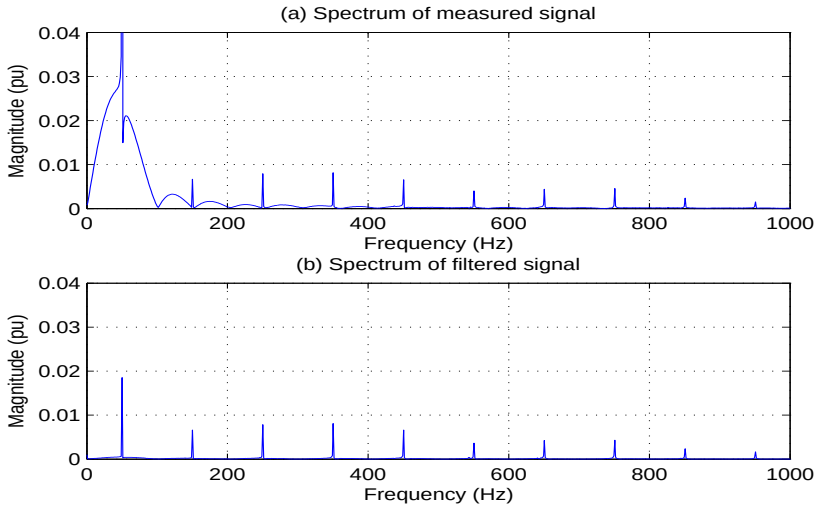

Figure 2: Spectra of the measured noise in 50-Hz voltage (correspond to Figure 1(a)) and the extracted noise (correspond to Figure 1(b)).

around the fundamental frequency disappear from the extracted noise due to the bandpass filter.

In order to quantify this realistic noise, a signal-to-noise ratio with a pure 50-Hz sine wave used as the reference signal is defined in (2).

$$SNR = 10 \log_{10} \frac{P_{signal}}{P_{noise}} \tag{2}$$

where P_{signal} and P_{noise} are the power of the reference sine wave and the extracted noise, respectively. In this study, a set of 366 voltage recordings are used to extract 366 noise realizations; and SNRs for these noise realizations are calculated according to (2) and presented in the histogram in Figure 3.

The histogram shows that the defined SNR for the extracted noise sequences (the original extracted noise without scaling, denoted by natural noise sequences) varies from 32 dB to 34 dB and the mean value is 33.17 dB.

4 Simulations and Results

In this part we present the evaluation results from the study for the Kalman filter, ESPRIT, MUSIC, and a segmentation algorithm.

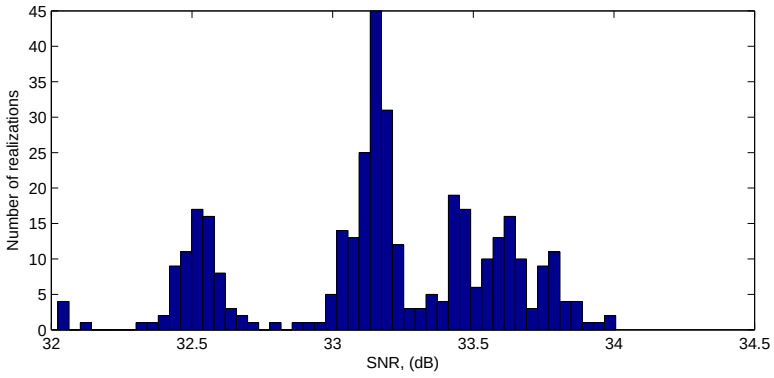

Figure 3: Histogram of SNRs of 366 extracted noise realizations.

4.1 Evaluate the impact of harmonic model order using Kalman filter-based estimation on quasi-stationary signals

The impact of model order on the performance of Kalman filters under the harmonic model on quasi-stationary signal is studied for two cases: one is for a clean synthetic voltage containing only the fundamental component, and another is a noisy semi-synthetic voltage obtained by superimposing the real measurement noise into the clean synthetic voltage. To quantify the performance, the rms error in (3) is used.

$$e_{rms} = \sqrt{\frac{\sum_{i=1}^{L}[s(i) - \hat{s}(i)]^2}{L}} \tag{3}$$

where $s(i)$ and $\hat{s}(i)$ are the i^{th} sample of the clean signal and the estimated signal, respectively, and L is the length of the signal. Figure 4 shows the rms errors as a function of the harmonic model order.

From Figure 4(a) one can see that the rms error for the clean signal reaches its minimum value at $K = 1$ since the signal only contains the fundamental component. In the case of using semi-synthetic data, the rms error in Figure 4(b) decreases with the increase of model order due to the fact that more harmonics in the noise are moved to the signal subspace. Although, in both cases, the rms errors are rather small, the error for a noisy voltage is a factor of 50 higher than the one for a clean synthetic voltage. The model order K, thus, in the case of application for quasi-stationary noisy signals can be freely selected depending on the number of harmonics to be estimated. The very high model order with heavy computational burden is not necessary if only several power harmonic components are of interest.

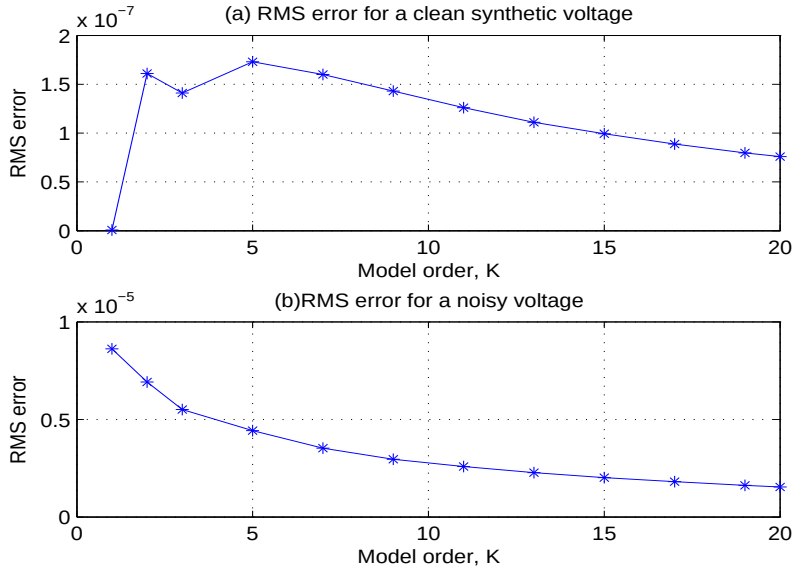

Figure 4: rms errors vs. model order. Note that there is a factor 50 difference in vertical scale between the two graphs.

4.2 Evaluate the performance of ESPRIT and MUSIC using semi-synthetic data

In order to evaluate the performance of ESPRIT and MUSIC, a synthetic signal consisting of two sinusoids (50 Hz, 1 pu and 150 Hz, 0.3 pu) is generated. The set of 366 extracted noise realizations are added to this synthetic signal to create a set of 366 semi-synthetic noisy signals for each selected SNR. These semi-synthetic sequences are then used to evaluate the harmonic model using ESPRIT and MUSIC algorithms. The means and the standard deviations of the estimated parameters from these 366 noisy signal with different noise levels (SNRs) are then calculated. The results for frequency estimation using the two algorithms are plotted in Figure 5 and Figure 6 for the 50-Hz component and the 150-Hz component, respectively.

From the figure, one can see that the estimated frequencies converge to the ground-truth frequencies with the increase of SNR (or the decrease of noise level). A systematic over-estimation is observed for MUSIC and a slight under-estimation is observed for ESPRIT. Table 1 shows the estimated parameters of the two algorithms at two selected noise levels: SNR $= \infty$ (no noise), and SNR $= 33.17$ dB (natural noise). In a similar way, amplitude estimation results are presented in Figure 7, Figure 8, and Table 2.

From the results, one can see that for the dominant fundamental component, the mean values tend to be stable at different noise levels but the standard deviations increase with increase of noise level. For the third harmonic component,

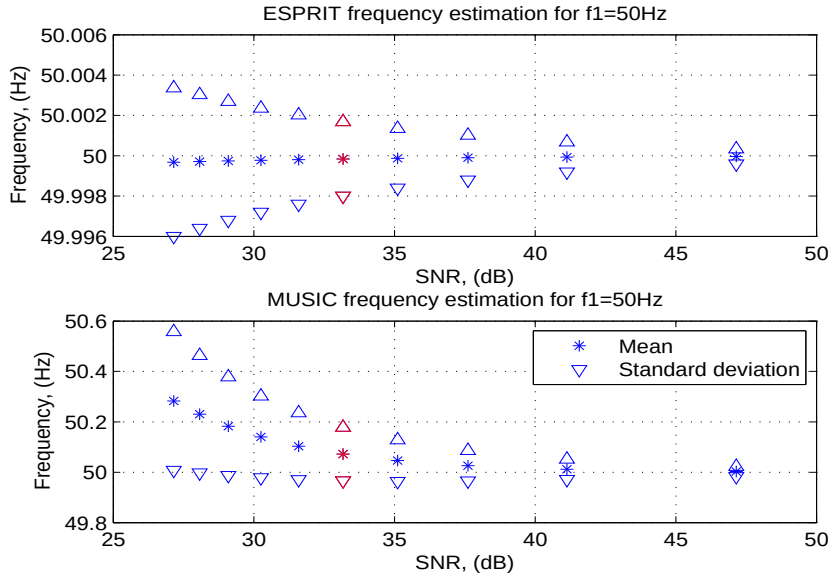

Figure 5: Frequency estimation results for the 50-Hz component. The red points represent the case of SNR= 33.17 dB which corresponds to the case the extracted noise is directly added to the synthetic signal (natural noise).

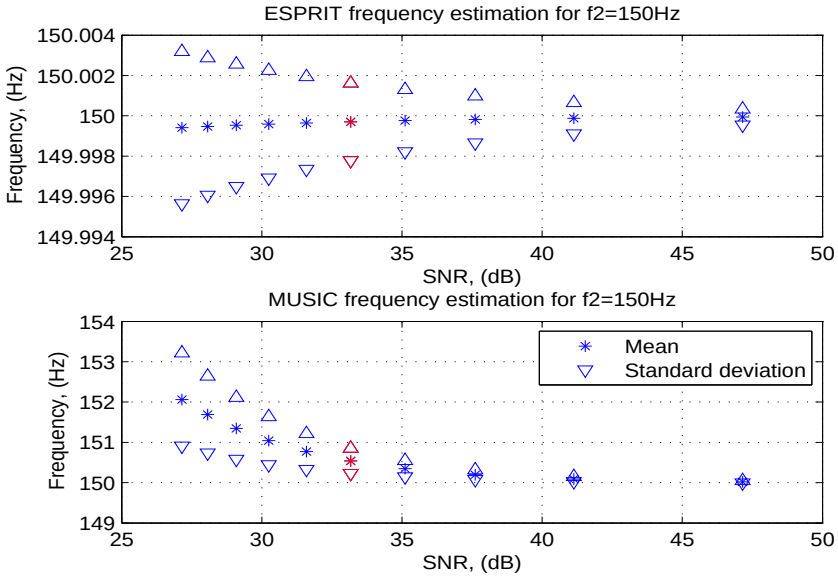

Figure 6: Frequency estimation results for the 150-Hz component.

Table 1: Frequency estimates for no-noise and natural-noise scenarios (μ: mean value; σ: standard deviation; f1, f2: frequencies).

	SNR=∞ (no noise)		SNR = 33.17 dB (natural noise)			
	f1	f2	$\mu(f1)$	$\sigma(f1)$	$\mu(f2)$	$\sigma(f2)$
MUSIC	49.99	149.99	50.08	0.12	150.92	0.32
ESPRIT	50.00	150.00	49.99	8e-4	150.00	7e-4

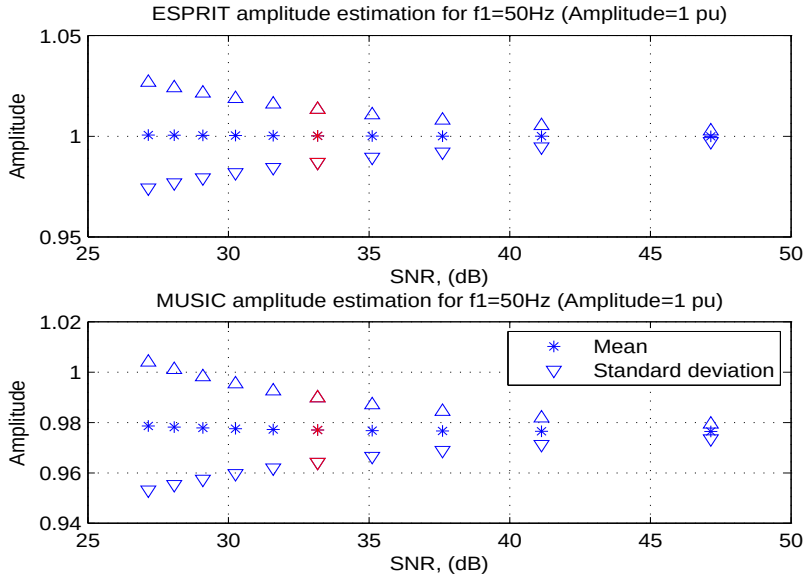

Figure 7: Amplitude estimation results for the 50-Hz component.

Table 2: Amplitude estimates for no-noise and natural-noise scenarios (μ: mean value; σ: standard deviation; A1, A2: amplitudes).

	SNR=∞ (no noise)		SNR = 33.17 dB (natural noise)			
	A1	A2	$\mu(A1)$	$\sigma(A1)$	$\mu(A2)$	$\sigma(A2)$
MUSIC	0.9765	0.318	0.9755	0.0130	0.3182	0.0024
ESPRIT	1.00	0.30	0.9984	0.0129	0.3018	0.0014

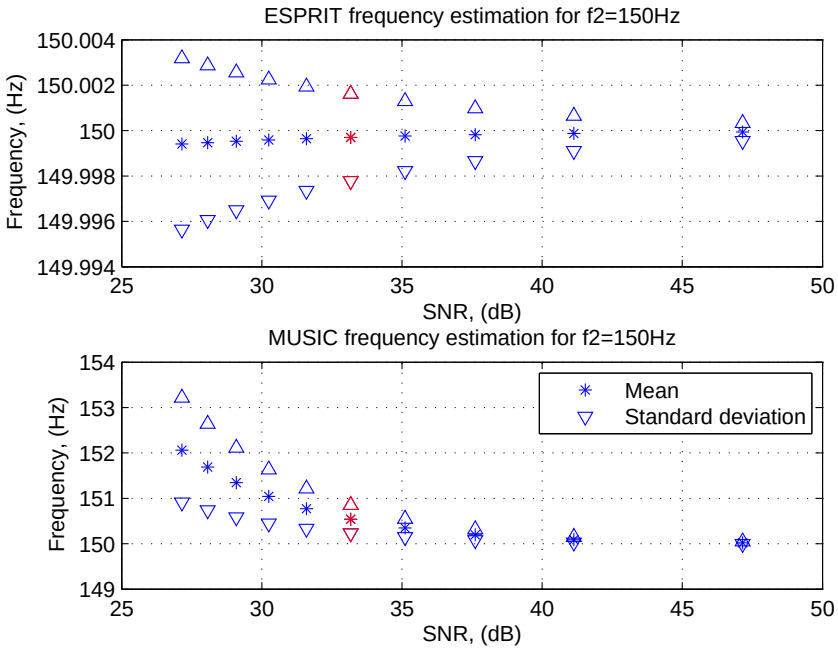

Figure 8: Amplitude estimation results for the 150-Hz component.

overestimation is observed for both algorithms. This is due to the contribution of the third harmonic component in the noise. MUSIC shows consistent underestimation for the dominant component and overestimation for the weak component.

In order to observe the performance at the natural noise scenario, the estimates of the two algorithms under this noise level for 366 realizations are presented in Figure 9, Figure 10. The estimates corresponding to the maximum error are given in Table 3.

Table 3: Frequency and amplitude estimates corresponding to the maximum error under natural noise scenario.

	f1	f2	A1	A2
MUSIC	50.56 (1.11%)	152.43 (1.62%)	0.957 (4.303%)	0.4265 (42%)
ESPRIT	49.98 (0.04%)	149.98 (0.01%)	1.022 (2.2%)	0.3067 (2.23%)

The results show that ESPRIT shows very good and stable performance over different noise realizations. The aim of this study is, however, not to compare

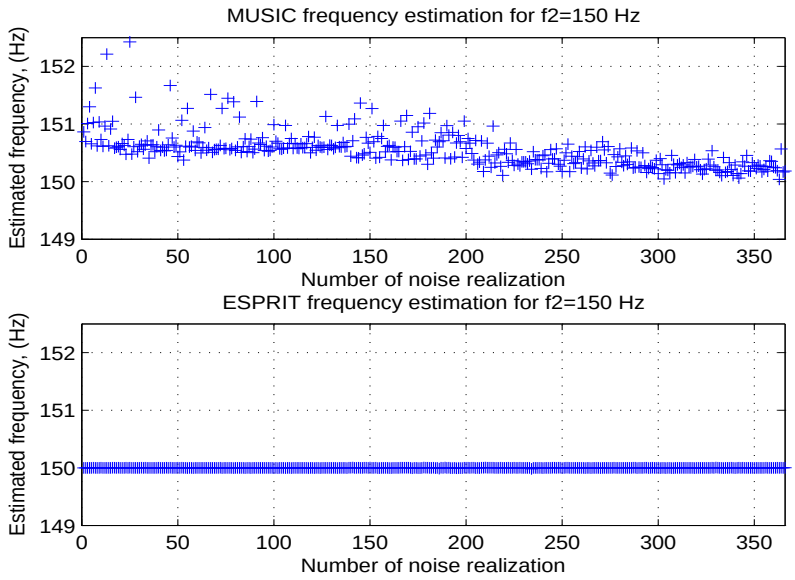

Figure 9: Frequency estimates of 150-Hz component at the natural noise level.

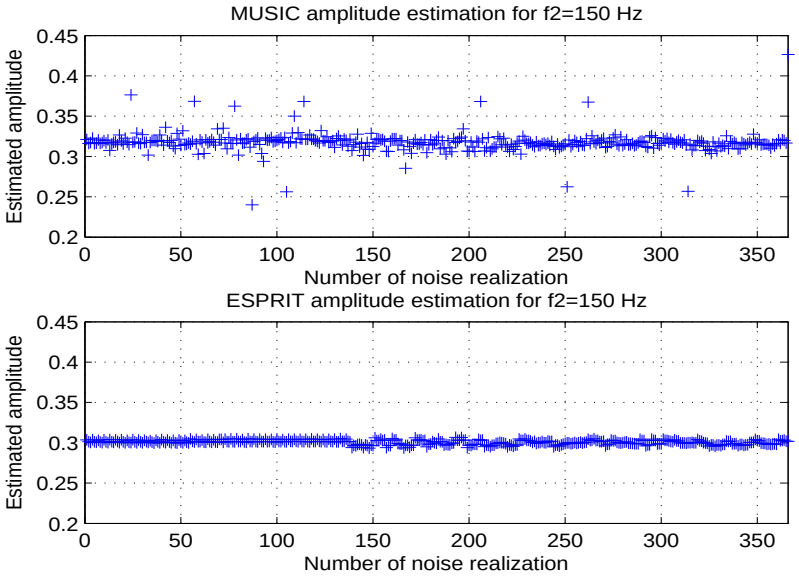

Figure 10: Amplitude estimates of 150-Hz component at the natural noise level.

the performance of the two algorithms as the settings for the two algorithms are different: the signal subspace dimension is half of the data length for ESPRIT and 10 (equal to the number of sinusoids to be estimated) for MUSIC. The aims are to illustrate the evaluation method using semi-synthetic data and to show that the performance of both ESPRIT and MUSIC is good enough under real power-system noise. Table 3 shows that ESPRIT gives very good performance at the natural noise level; the maximum error is 0.04% for frequency estimation and 2.23% for amplitude estimation. MUSIC gives higher error in most of the cases and the maximum error is observed for the case of amplitude estimation for the weak signal. This is due to the quite low signal subspace dimension setting.

4.3 Evaluate the performance of segmentation algorithm

The proposed evaluation method is also applied to the segmentation algorithm proposed in [9]. This segmentation algorithm calculates a forward (causal) and backward (anti-causal) version of the Kalman filter residuals to very accurately detect the location of transition segments. For the purpose of this study, the set of 366 extracted noise realizations is added to a synthetic fast transition obtained by multiplying a sine wave with a step transition at time T_0 to create 366 transition sequences. The next step is to apply the segmentation algorithm to these sequences to evaluation its performance. The difference (error E) between T_0 and the estimated transition instant ($\hat{T}_0$) is used to evaluate the performance. In the case of no noise, the error E is 5 samples (0.5 ms as the sampling frequency is 10 kHz). The evaluation results are shown in Figure 11.

The top plot in Figure 11 shows that the mean error in most of the cases are very close to 5 samples which is the error of the case of no noise. The standard deviations show systematic decrease with increase of SNR. The estimates in the case of natural noise are presented in the bottom plot of Figure 11 which vary from 2 samples to 8 samples. The results show that the segmentation algorithm is not significantly impacted by the presence of noise. In contrast, the presence of noise somewhat reduces the estimation error; this is due to the fact that when the noise increases, the model unfit increases which leads to increases in the detection parameter making it easier to detect the transition point. However, this does not imply that the overall performance of the segmentation algorithm is better with the presence of noise. At higher noise levels, the possibility of false alarm increases (Reference [9] is recommended for complete understanding of this issue).

5 Conclusion and Future Work

A systematic method has been proposed to evaluate the performance of signal-processing techniques in power-system applications. The method combines syn-

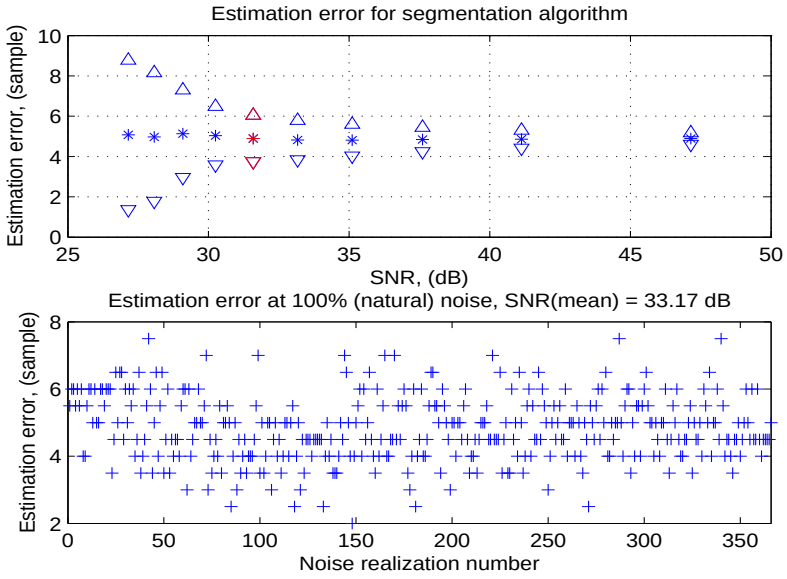

Figure 11: Estimation errors for segmentation algorithm.

thetic signals with a large number of measured noise realizations. The method is motivated by the real world scenarios of non-white noise, where we propose to use synthetic data embedded in measurement noise to make the data close to the real world situation. Since non-white noise does not fit to the white noise assumption in the harmonic model, performance evaluation is conducted and shown in this paper in terms of mean and variance of the estimation under different estimation techniques in several applications. This evaluation method could be used to evaluate the performance of any estimation techniques applied to power-system voltages and currents.

The study shows that the algorithms behave differently under measured noise. In the case that Kalman filter is applied to quasi-stationary signal under harmonic models, the rms errors between the input and the estimated signals are rather small. If a few harmonics of power frequency are interested, it is not necessary to have high model order to reduce computational load. Further, mean estimates and standard deviations for semi-synthetic sequences under different SNRs and realizations are studied to show the impact of measured noise in power systems on the performance of ESPRIT and MUSIC algorithms. The results show that both ESPRIT and MUSIC give estimations with acceptable error under natural noise scenario and their application to power-system data is still feasible. In the case of evaluation of the segmentation algorithm, the influence of the measured noise on the performance of the algorithm is not significant. The study presented in this paper has also shown that it is possible to evaluate signal-processing algorithms under realistic noise situations and that such an evaluation provides additional

information beyond evaluating using white noise.

A large number of noise realizations have been used in this study to evaluate the algorithms but they all are collected from one measurement point. It is more interesting to observe the performance of the algorithm subjected to noise sequences obtained from various locations and voltage levels. Another issue to study next is to look at the influence of the broadband components around the fundamental frequency by applying different filtering techniques to remove the fundamental frequency.

References

[1] M. H. J. Bollen and I. Y. H. Gu, *Signal processing of power quality disturbance*, A John Wiley & Sons, Inc., 2006.

[2] A. Testa, M.F. Akram, et al., "Interharmonics: Theory and Modeling," *Power Delivery, IEEE Transactions on*, vol. 22, no. 4, pp. 2335-2348, 2007.

[3] M. H. Hayes, *Statistical Digital Signal Processing and Modeling*, A John Wiley & Sons, Inc., 1996.

[4] T. Zheng, X. Yang, et al., "Research of noise characteristics for 10-kV medium-voltage power lines," *Power Delivery, IEEE Transactions on*, vol. 22, no. 1, pp. 142-157, 2007.

[5] A. Tjäder, I. Y. H. Gu, et al., "Performance evaluation for frequency estimation of transients using the ESPRIT: measure noise versus white noise," 13^{th} *Int. Conf. Harmonics and Quality of Power (ICHQP)*, Wollongong, NSW, 2008.

[6] A. Paulraj, R. Roy, et al, "Estimation of signal parameters via rotational invariance techniques - Esprit," *Circuits, Systems and Computers,* 19^{th} *Asilomar Conference on*, 1985.

[7] I. Y. H. Gu and M. H. J. Bollen, "Estimating interharmonics by using sliding-window ESPRIT," *Power Delivery, IEEE Transactions on*, vol. 23, no. 1, pp. 13-23, 2008.

[8] R. Schmidt, "Multiple emitter location and signal parameter estimation," *Antennas and Propagation, IEEE Transactions on*, vol. 34, no. 3, pp. 276-280, 1986.

[9] C. D. Le, I. Y. H. Gu, and M. H. J. Bollen, "Joint causal and anti-causal segmentation and location of transitions in power disturbances," *IEEE PES General Meeting*, Minneapolis, USA, 2010.

[10] T. Parks and J. McClellan, "Chebyshev approximation for nonrecursive digital filters with linear phase," *Circuit Theory, IEEE Transactions on*, vol. 19, no. 2, pp. 189-194, 1972.